

Finite element modeling of CFRP composite tubes under low velocity axial impact

Dora Karagiozova¹ | Pouria B. Ataabadi² | Marcilio Alves² 

¹Institute of Mechanics, Bulgarian Academy of Sciences, Sofia, Bulgaria

²Group of Solid Mechanics and Structural Impact, Department of Mechatronics and Mechanical Systems Engineering, University of São Paulo, São Paulo, Brazil

Correspondence

Marcilio Alves, Group of Solid Mechanics and Structural Impact, Department of Mechatronics and Mechanical Systems Engineering, University of São Paulo, São Paulo 05508900, Brazil.
 Email: maralves@usp.br

Funding information

Science and Education for Smart Growth Operational Program (2014–2020) and co-financed by the European Union through the European Structural and Investment funds, Grant/Award Number: BG05M2OP001-1.001-0003-C01; CNPq, Grant/Award Number: 401092/2014-3

Abstract

The dynamic axial crushing response of circular tubes made of unidirectional carbon fiber-epoxy composite was investigated numerically applying a new approach to the modeling of the delamination process. In the proposed approach, delamination (interface damage) was modeled by inserting isotropic resin plies capable of damage. They are tied to the adjacent laminae and replace the commonly used surface-based cohesive model. Two multi-layer models of laminated tubes having cross-ply and angle-ply stacking sequences were simulated using stacked conventional shell elements layers to capture the crushing response and intralaminar and interlayer damage of laminated tubes. The progressive failure analysis in Abaqus/Explicit was utilized to model the successive damage of both the interface and laminae. Both the intralaminar layers and isotropic resin layers were modeled by the conventional reduced integration shell element (S4R). The suggested modeling technique offers some advantages compared to the main-stream interface modeling of the axial impact of laminated tubes. The computational cost is reduced and yet accurate predictions are obtained. The FE models based on the proposed delamination approach were validated by experimental test results obtained by the authors for cross-ply and angle-ply tubes subjected to a low-velocity impact.

KEY WORDS

dynamic effects, interface modeling, laminated composite tubes, low-velocity axial impact, ply layout effects

1 | INTRODUCTION

Composite materials play a key role in the crashworthy design of many transportation systems where crash safety and weight are both critical parameters. Numerous experimental investigations have been conducted in order to analyze the crushing performance of composite absorbers with different cross-sections, such as circular, square, and open section geometries aiming at the replacement of the metallic energy absorber used in the aerospace and automotive industries. The kinetic energy

absorbers in automobile and aircraft structures are subjected to loads with various characteristics, including different loading rates, initial kinetic energy and loading direction affecting their energy absorption performance. Furthermore, the structural response of the laminated composites depends on the composition of their constituent materials, such as fiber volume fraction, fibers orientation, stacking sequence. The various combinations of the above parameters make the experimental optimization of the composite absorbers more costly than the current design of metallic ones.

Analytical models developed to predict the energy absorption of laminated composite tubes (eg, Mamalis et al^[1]), although with good accuracy, have limited applications due to the necessary simplifying assumptions related to the high complexity of the problem. The finite element analysis has been recognized as a powerful and advantageous modeling tool in many engineering applications, including the response analysis of composite structures to dynamic loading. Commercial finite element packages, such as LS-Dyna, Abaqus, and PAM-CRASH have been widely used for the prediction of the crushing behavior of composite structures under quasi-static and impact loading.

Two major approaches have been used to model the performance of laminated structures: (i) single-layer model and (ii) multi-layered model. The simplified single-layer model of a laminated tube cannot model delamination and an appropriate material calibration along with a homogenization procedure is required to predict the force-displacement characteristic. This approach could be useful for more ductile composite materials that exhibit progressive folding under axial compression (Morthorst and Horst^[2]). The multi-layer approach has received more attention since the layer-wise nature of this approach is capable of modeling both intralaminar and interlaminar behavior of laminated composite parts. However, the interface modeling brings extra challenges and makes the multilayer modeling approach more complex. A comprehensive review of the analysis strategies related to a low-velocity impact of laminates at a structural level leading to a good balance between accuracy and computational efforts is given by Bogenfeld et al.^[3] It is worth mentioning the damage and delamination models of the transverse impact on laminated plates developed by Shi et al.,^[4] Feng and Aymerich,^[5] and Liu et al.^[6] They used brick elements for the composite and cohesive elements for the interface. Continuum shell elements and cohesive interface elements were utilized by Riccio et al^[7] to model the dynamic progressive failure of laminated plates under a low-velocity transverse impact. The deformation is localized in a relatively small domain of the plates allowing refined mesh and accurate results.

A simplified material degradation approach was proposed by Wang et al^[8] to describe damage of laminated plates under transverse low velocity impact including delamination failure in tension and compression. A progressive failure methodology was presented by Donadon et al^[9] for modeling composite structures under impact loading. The accuracy of the proposed 3D failure model, which is based on continuum damage mechanics, was verified by experimental tests in different static and dynamic loading regimes. The example of a transverse impact loading on a woven composite plate served as

validation of the proposed methodology. Various aspects of modeling low velocity transverse impact were discussed in.^[10-15] The validity of several techniques for modelling a transverse impact was analyzed by Khalili et al.^[10] when focusing on the finite element type, impactor model, and solver type. Tita et al^[11] and Sellitto et al^[12] show that the 3D stress state of the solid elements gives more accurate predictions of the experimental tests in comparison with models with shell elements.

Since the laminated tubes are likely to undergo significant bending deformation under impact loading (Ataabadi et al^[16]), the finite elements used to model these structures should be capable of capturing bending correctly (Bogenfeld et al.^[3]). Thus, mid-surface shell elements with six DOFs (three rotational and three transitional DOFs at each node) are promising candidates to model the intra-ply behavior. However, it is observed that the conventional shell elements with the mid-surface formulation (S4R shell element) in Abaqus have been rarely used (Zhu et al^[17] and Zhao et al^[18]) to build multi-layer FE models of laminated tubular structures under axial impact loading. In contrast to this, the mid-surface shell elements in LS-Dyna have been widely used to simulate the multi-layer composite parts under an axial impact (Morthorst and Horst,^[2] Mamalis et al.,^[19] Huang and Wang,^[20] McGregor et al.,^[21] Siromani et al.,^[22] McGregor et al.,^[23] Reuter et al.^[24]).

The surface-based cohesive model (CZS) interaction in Abaqus is a promising technique to bond adjacent laminae. No extra elements are required to represent the interface layers and such finite element models would be computationally efficient, particularly for relatively large structures undergoing damage within a large domain. However, the major complexity of modeling delamination of axially loaded tubes comes from the development of the buckling modes with different displacement magnitudes of the individual composite layers depending on their stiffness (thickness and lay-up). The CZS technique in Abaqus is based on a master-slave contact algorithm so that the accuracy of the model depends also on the contact behavior of the bonded elements. Since the surface-based cohesive model does not assume an initial tie connection between the layers, the use of equal elastic constants and critical stresses for the whole model can lead to premature delamination. This process can start from two neighboring plies with a relatively large difference in the buckling displacement magnitudes, which will initiate delamination locally. Then, delamination between the affected layers develops rapidly causing a premature stiffness reduction of the entire model. This contact problem for axial compression of tubes leads to large and physically unrealistic delamination leading eventually to a premature structural instability predicted by the model (Bogenfeld et al^[3]). This phenomenon is

well observed for conventional shell element (S4R or S4) under compressive load due to a poor contact response of these elements. Therefore simulations that used the S4R element together with the CZS in Abaqus have been seldom reported for structures undergoing axial compressive loading. Very few successful multi-layer models using CZS and conventional shell element (S4R) have been built when using Abaqus (Dlugosch et al^[25]) for composite tubes under axial impact. For example, the above-described contact problem for axially loaded laminated structural members has been solved in LS-Dyna by the tiebreak contact formulation, which was predominantly utilized to bond the mid-surface shell elements to model multi-layer composite absorbers under axial impact.

A few researchers (Zhu et al^[17] and Zhao et al^[18]) have built models of laminated tubes under axial impact using tied S4R elements and element-based cohesive zone model (CZE) in Abaqus. However, the CZE requires extra continuum elements to represent the interface between laminae, which significantly increases the computational cost.

Continuum shell elements (SC8R) and conventional shell elements (S4R) have a similar formulation.^[22] However, the continuum shell element discretizes the whole continuum body and has better contact behavior. Therefore, models comprising a continuum shell and CZS bonding contact formulation have shown a more stable response under compressive loading than the S4R element (Bogenfeld et al^[3]). This response characteristic is related to the better contact behavior of the continuum elements. Therefore continuum shell elements have been often used to model multi-layer laminated tubes under an axial impact (Palanivelu et al,^[27] Patel et al,^[28] Sokolinsky et al^[29]). However, thin continuum shell elements may result in a small stable time increment in Abaqus/Explicit, particularly for thin shell applications (like composite laminae) thus increasing significantly the number of increments taken to complete the analysis when compared to the same problem modeled with conventional shell elements.^[26]

It is also possible to incorporate three-dimensional solid elements with one layer of bricks representing a ply of composite material. However, several elements through the thickness should be used to capture correctly the lamina bending response (Matthews et al^[30]). For example, Chiu et al^[31,32] and Tan et al^[33,34] have used solid elements to represent the composite plies with three solid elements through the thickness in composite absorbers under axial compression. Such models for relatively large-size structures are computationally inefficient. Moreover, in theory, the technique of layering brick elements through the thickness of the relatively thin plate or shell leads to ill-conditioned sets of equations (Matthews

et al^[30]). The three-dimensional solid elements are more suitable when the composite lay-up is thick and the geometry is more solid-like than shell-like and a detailed 3D stress field analysis in the material is required. It is important to note that the global response in terms of force-displacement characteristic, without a detailed stress analysis, does give sufficient information about the structural performance, as reported in most publications relevant to the axial impact on composite components. Therefore, elements with mid-surface formulation are more suitable for this type of simulation.

The present study aims to investigate the performance of the conventional shell elements (S4R) in modelling intra-ply (lamina) behavior of laminated tubular absorber under axial compressive dynamic load. In-built progressive failure analysis (PFA) in Abaqus based on Hashin's failure theory is used to model the intra-laminar behavior of composite laminae. A new approach is proposed to model the delamination process instead of using the mainstream bonding techniques, CZE and CZS available in Abaqus/Explicit. In the proposed model, a thin layer of conventional shell elements with isotropic mechanical properties (epoxy resin) was inserted between every two laminae, which were tied to this thin isotropic layer in order to provide adhesion between the laminae. The delamination then is modeled by the degradation of the epoxy resin when using a suitable built-in progressive failure model available in Abaqus material library.

The proposed approach takes the advantage of using the computationally less expensive conventional shell elements in comparison to continuous shell elements for axial buckling problems where a sufficient number of the latter elements are required to represent bending with large curvature. The disadvantageous property of poor force transfer between two layers of conventional shell elements representing the neighboring composite layers, when using a surface-based cohesive approach, is compensated by the additional resin layer tied to each two composite layers. From an engineering viewpoint, the resin layer can be considered as a replacement of the considerably more expensive cohesive elements. The use of shell elements with resin properties also eliminates the cumbersome (and in some cases artificial) selection of the parameters of the traction separation law for the cohesive surface interaction. Besides, together with the commonly analyzed stress and strain normal and tangential to the neighboring composite layers, the inserted resin layers can more adequately represent the stress-state of a structure under axial compression where the compression stresses and strains play an important role for the critical conditions for delamination.

The proposed approach is currently oriented to the modeling of axially compressed structures. The FE

models based on this delamination approach were validated by experimental test results obtained by the authors for cross-ply and angle-ply tubes subjected to a low-velocity impact.^[16]

2 | FINITE ELEMENT MODEL DESCRIPTION

The commercial software package Abaqus/Explicit is used to build FE models for cross-ply and angle-ply CFRP tubes. Typical FE models are presented in Figure 1(A),(B) showing a full tube and 1/4 tube model, respectively. The tube with high L was sandwiched between two rigid surfaces. All degrees of freedom of the bottom surface were constrained while the upper surface was allowed to move only in the axial direction (z -direction). A point mass was attached to the reference point $(0, 0, L)$ of the upper surface to represent the impact mass used in the tests. No constraints on the degrees of freedom were imposed on the elements' nodes in contact with the rigid surfaces. Symmetry boundary conditions were imposed on the composite and resin layers in the (x, z) and (y, z) planes for the 1/4 tube model as shown in Figure 1(D). Details of the 45° chamfer used as a trigger in all models are shown in Figure 1(C). It was found from the drop test results^[16] that the chamfer angle has no significant effect on the mean force of the laminated tubes so that no other

chamfer angles were modeled. The geometric parameters of the tubes from Reference [16] used to validate the proposed modeling approach are given in Table 1. It was observed during the tests that delamination and damage of the tube develop within a narrow zone in the loading direction, which is comparable with the tube thickness, while the stationary end was not affected by delamination or damage. Besides, the force-displacement curves possessed a notable uniformity. Due to this reason, models with a shorter length than the tested specimens with a typical length of 100 mm^[16] were built in order to reduce the computational time for model validation. Models with tube lengths $L = 65$ mm for the full tube and $L = 70$ mm for the 1/4 model are used.

Conventional shell elements S4R are used to model the composite layers with the corresponding fiber orientations (marked as L1, L2, and so forth, in the models). The material properties of the unidirectional prepreg used in the tubes^[16] are given in Table 2. The majority of the mechanical characteristics of the tested composite materials, such as E_1 , E_2 , G_{12} , ν_{12} , X^T and S were also obtained by the present authors in^[35] demonstrating a very close agreement with the material data provided by the manufacturer. The layers' delamination is modeled by introducing thin layers of epoxy resin between the composite layers as it is further described in Section 2.2. The adhesive epoxy layers are also discretized by S4R shell elements and marked as C1, C2, and so forth, in all

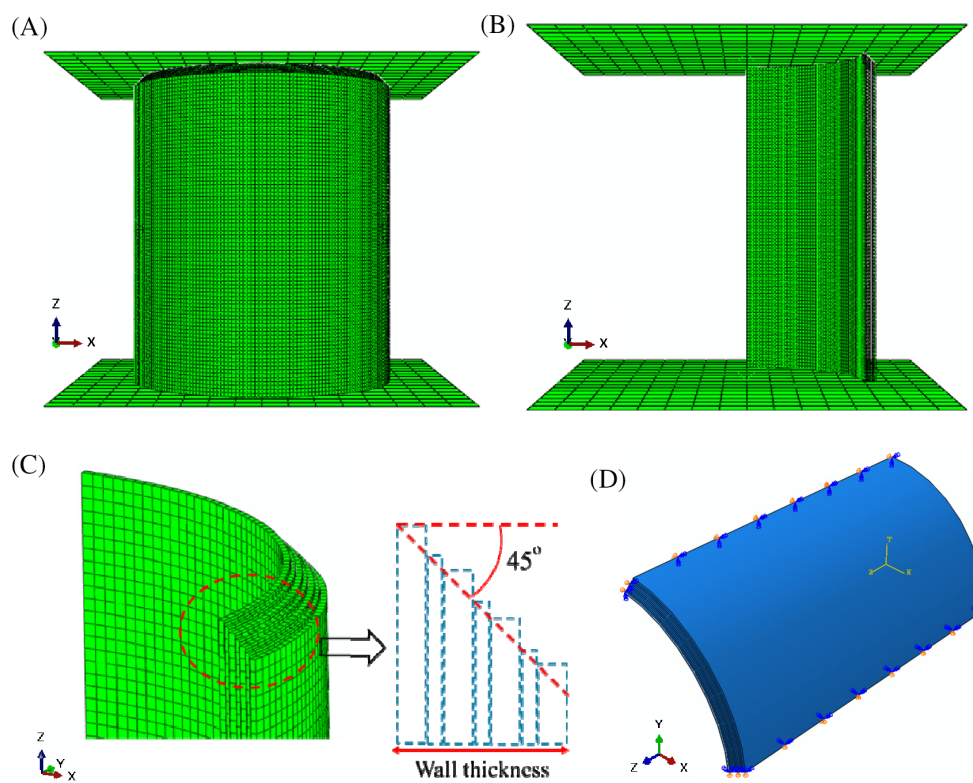


FIGURE 1 Initial geometry of the models; (A) A full tube model; (B) 1/4 model; (C) Details of the external chamfer modeled with “stepped length geometry”; (D) Symmetry boundary conditions of the 1/4 model [Color figure can be viewed at wileyonlinelibrary.com]

TABLE 1 Tubes' geometry^[16]

Item	Tube configuration (a)	Tube configuration (b)
Stacking sequence ^{a,b}	(±45/0/±45/0/±45/0/±45)	(0/(90) ₂ /0) _s
Inner diameter (mm)	50.00	50.00
Outer diameter (mm)	54.70	54.38
Cross-section area (mm ²)	386.1	353.1
Mass per length (g/mm)	0.592	0.542
Short reference name	(±45/0...) or angle-ply	(0/90...) or cross-ply

^a0°, ±45°, and 90° are measured from the tube axis.

^bBold layers are 300 gsm Unidirectional (0.3 mm thick) and the others are 200 gsm Unidirectional (0.2 mm thick).

TABLE 2 Nominal mechanical properties of CF/Epoxy lamina, as provided by the manufacturer, CFT Company and obtained by the present authors^[35]

Property	Symbol	Units	Unidirectional preprep	
			CFT Company	Ref. [35]
Elastic modulus 0°	E_1	GPa	135	136.32
Elastic modulus 90°	E_2	GPa	10	9.30
In-plane shear modulus	G_{12}	GPa	5	5.10
Major Poisson's ratio	ν_{12}	—	0.3	0.294
Ultimate tensile strength 0°	X^T	MPa	1500	1550
Ultimate tensile strength 90°	Y^T	MPa	50	—
Ultimate compressive strength 0°	X^C	MPa	1200	—
Ultimate compressive strength 90°	Y^C	MPa	250	—
Shear strength	S	MPa	70	73.60

Note: UD ply density is 1600 kg/m³.

TABLE 3 The thickness of the composite plies and the associated fiber orientations of the FE tube models

Cross-ply models							
CP-M1	L1	L2	L3	L45	L6	L7	L8
	0/0.3 mm	90/0.3 mm	90/0.3 mm	0/0.4 mm	90/0.3 mm	90/0.3 mm	0/0.3 mm
CP-M2	L1	L23	L45	L67	L8		
	0/0.3 mm	(90) ₂ /0.6 mm	0/0.4 mm	(90) ₂ /0.6 mm	0/0.3 mm		
CP-M3	L1	L23	L45	L67	L8		
	0/0.3 mm	90/0.6 mm	0/0.4 mm	90/0.6 mm	0/0.3 mm		
Angle-ply models							
AP-M1	L1	L2	L3	L4	L5	L6	L7
	±45/0.4 mm	0/0.26 mm	±45/0.4 mm	0/0.26 mm	±45/0.4 mm	0/0.26 mm	±45/0.4 mm
AP-M2	L1	L2	L3				
	(±45,0)/ (0.4,0.26)mm	(±45,0, ±45)/ (0.4,0.26,0.4)	(0,±45)/ (0.26,0.4)mm				
AP-M3_1/4	L1	L2	L3	L4	L5	L6	L7
	±45/0.4 mm	0/0.26 mm	±45/0.4 mm	0/0.26 mm	±45/0.4 mm	0/0.26 mm	±45/0.4 mm

models. The general contact formulation available in Abaqus/Explicit with a friction coefficient of 0.3^[1] was used to model the contact between all parts of the model.

No data are available for the dynamic effect on friction so that the static friction coefficient with the penalty formulation was used.

A fully fixed rigid plate is used to support the tube at the stationary end ($z = 0$). All degrees of freedom of the upper rigid plate at $z = L$ are also fixed except for the displacement degree in the direction of loading. The impactor is modeled as a point mass attached to the reference point of the upper plate with a prescribed initial velocity.

Models with a different number of inserted epoxy layers are constructed in order to examine the influence of the cross-section discretization on the delamination process as well as on the force-displacement characteristics of the laminated tubes. The geometric characteristics of the analyzed tube models are described in Table 3. Models CP-M1, CP-M2, and CP-M3 refer to full cross-ply tubes, AP-M1 and AP-M2 refer to the full angle-ply tubes while AP-M3_1/4 is a $\frac{1}{4}$ angle-ply model with the same ply configuration as those in AP-M1. The layer's characteristics in Table 3 are defined as "ply orientation/layer thickness." For example, "0/03 mm" denotes a 0.3 mm thick ply with 0° fiber orientation. The notation (90)₂ in model CP-M2 refers to a two-ply model without allowing delamination between these two plies to occur before damaging any of the plies. The layer thicknesses are calculated to match as close as possible the nominal thicknesses of the cross-sections on the tested tubes.^[16]

2.1 | Intralaminar damage model

Orthotropic material properties are assigned to each UD composite lamina according to the fiber orientation by using a pre-defined local coordinate system. The Hashin's 2D failure criterion^[36] is applied to the composite layers to predict the matrix and fiber failure. The model formulation is available in Abaqus documentation.^[37] The material parameters used in the present simulations are given in Table 2. Damage evolution was controlled by the energy criterion with a linear law.^[37] The values of the corresponding energies G_{FT}^C , G_{FC}^C , G_{MT}^C and G_{MC}^C dissipated during damage for fiber tension, fiber compression, matrix tension, and matrix compression failure modes, respectively, are given in Table 4. Element removal takes place when the damage parameter $D = 0.98D_{max}$ ($D_{max}=1$ ^[37]). Since the damage model is mesh dependent, models with different element sizes were simulated,

with the results from the mesh sensitivity analysis presented in Appendix 0. It was established that S4R shell elements with an average side length of 0.75 mm give sufficiently accurate predictions for the response of the examined cross-ply and angle-ply tubes.

It has been established that the impact attenuators made of carbon fiber reinforced plastic exhibit high load carrying capacity with high energy absorption however the failure mode is brittle with debris formation.^[38] Therefore the fracture energy in the fiber direction, as well as friction in the system, are among the major model parameters which influence the prediction of the load-bearing capacity of composite components and their increase leads to higher values of the anticipated specific energy absorption. It should be emphasized, however, that there is no general agreement with respect to the reported fracture energies in the literature where some researchers use fracture energies which are about five times larger than the energy at the damage initiation. These values result in much larger final strains than the experimentally measured ones. For example, Shi et al^[39] used values of 91.60 and 79.9 N/mm for tensile and compression fracture energies while Zhang et al^[40] used 10 and 10 N/mm for fracture energies in the fiber direction for the same composite material. The energies related to damage evolution in the present study are calibrated to obtain final strains, which are approximately twice the strains at damage initiation. Simulations of the tensile tests of angle-ply and cross-ply coupons^[35] were carried out to validate material model parameters together with the assumed energy for damage evolution (see Appendix 0).

2.2 | Interlaminar damage model

The cohesive contact behavior defined in Abaqus/Explicit is a convenient approach to model a bonded surface when the interface thickness is negligibly small. In this case, the macroscopic material properties of the glue material are not so relevant and the analysis must resort to concepts derived from fracture mechanics in terms of energy release rate. The delamination at interfaces is modelled in terms of traction vs separation in the three-

TABLE 4 Damage parameters for composite plies, Hashin damage model ($\alpha = 1$)

Damage initiation	X^T (MPa)	X^C (MPa)	Y^T (MPa)	Y^C (MPa)	$S^L = S^T$ (MPa)
	1500	1200	50	250	70
Damage evolution element	G_{FT}^C (mJ.mm $^{-2}$)	G_{FC}^C (mJ.mm $^{-2}$)	G_{MT}^C (mJ.mm $^{-2}$)	G_{MC}^C (mJ.mm $^{-2}$)	
	19.0	12.0	0.9225	5.43	

dimensional problems, the traction-separation-based model assumes three components of separation - one normal to the interface and two parallel to it when the corresponding stress components are assumed to be active at a material point.^[26] The stresses for surface-based cohesive behavior are defined as the cohesive forces acting along the contact normal and shear directions divided by the current area at each contact point.

The above approach can be used for problems in which the mixed-mode ratio has a weak dependence on the load. On the other hand, buckling, which is involved in the response of tubular structures to axial impact, is a highly nonlinear phenomenon, so that the mixed-mode ratio at a given point can change as the loading increases.^[41] The accurate evaluation of the energy release, in this case, is difficult as the stress components can vary from compressive to tensile combined with shear. This response type brings additional complexity to the delamination modelling of composite components under axial impact along with the poor contact formulation for the S4R elements.^[26] The difficulties in modelling the adhesive layers in hybrid FRP-metal tubes under axial compression were also mentioned by Dlugosch et al.^[25]

It should be also pointed out that the elastic behavior in the available traction-separation models in Abaqus is written in terms of an elastic constitutive matrix that relates the normal and shear stresses to the normal and shear separations across the interface. However, the components of the stiffness matrix have no direct relation to the properties of the actual adhesive material and it could be a cumbersome

task to define the values of these components in order to achieve an optimal performance of the FE model.

The development of different buckling modes of composite layers built of conventional shell element (S4R) and initially connected via cohesive surface (CZS) contact formulation makes the modelling of axially compressed tubes difficult when using the Abaqus/Explicit software. The computational efficiency of this combination, however, encourages one to apply modifications to such that model. For instance, González et al^[42] instead of applying the cohesive surface model between two adjacent S4R layers, first tied S4R layers to layers of surface elements. Then the cohesive surface model was applied to the surface element layers but not directly to the S4R element. In the latter study, low-velocity impact on the laminate plate was investigated and good results have been reported.^[42]

Using the idea of adhesive epoxy layers, an alternative approach to the modelling of the interfaces' behavior in laminated tubes is proposed here in order to accurately model the delamination of axially loaded tubes at a relatively low computational cost. Thin epoxy layers are

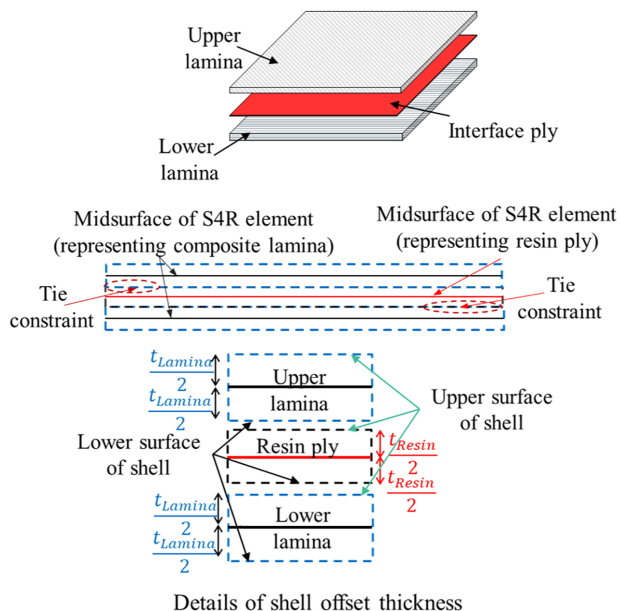


FIGURE 2 A general overview of the multi-layer approach in the present study [Color figure can be viewed at wileyonlinelibrary.com]

TABLE 5 A general overview of the material model for epoxy resin in the present study

Material model parts	Description	Input data
Undamaged response	Elastic (Isotropic behavior)	<ul style="list-style-type: none"> Elastic modulus Poisson's ratio
Damage initiation criterion	Ductile damage criterion + Isotropic plastic hardening	<ul style="list-style-type: none"> Tabular yield stress - plastic strain Triaxiality
Post-damage response	Damage evolution	<ul style="list-style-type: none"> Linear fracture energy

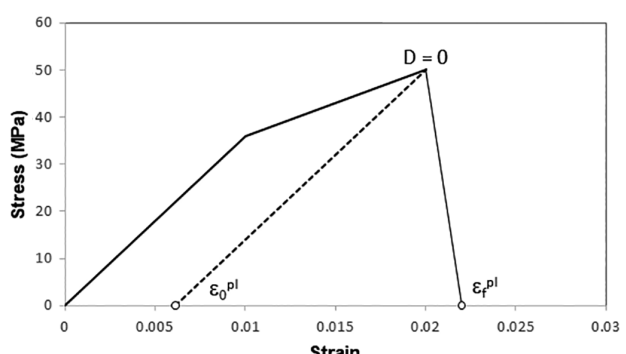
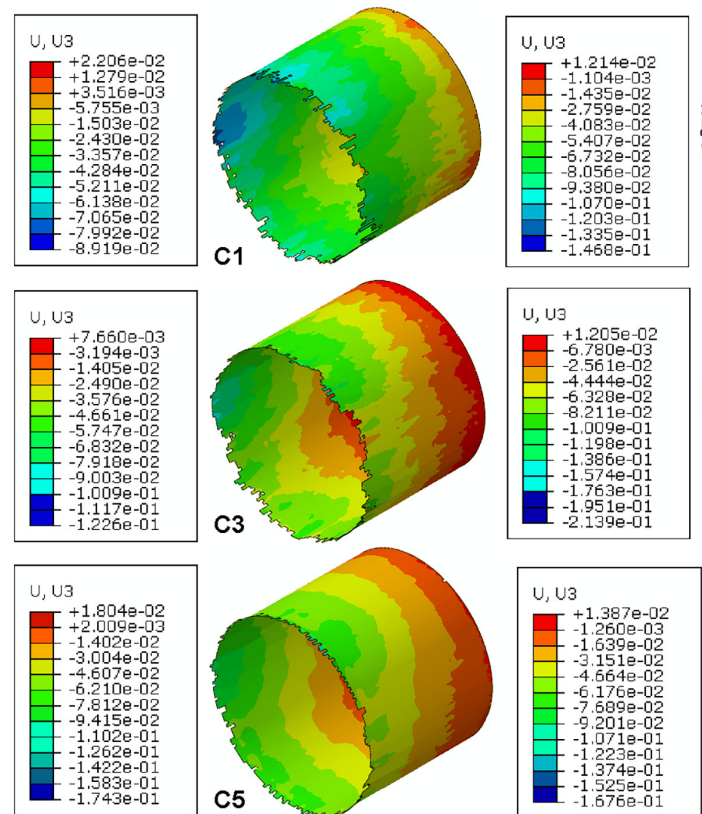


FIGURE 3 Stress-strain characteristic of the epoxy material used in adhesive layers

TABLE 6 Experimental results from the dynamic crushing tests.^[16]

Tests	Initial velocity (m/s)	Mass of the striker (kg)	F_{\max} (kN) (Mean)		F_{ave} (kN) (Mean)	
			DA45#	DC45#	DA45#	DC45#1
Dynamic set#1	6.72 ± 0.40	102 ± 0.2	60.78	56.77	34.05	31.00
Dynamic set#3	5.01 ± 0.20	205.20 ± 0.2	80.05	87.43	32.92	31.03
Dynamic set#4	9.62 ± 0.31	48.60 ± 0.2	71.88	61.62	35.24	30.93



inserted between the CFR composite layers as shown in Figure 2.

Due to the small thickness and small strength, the inserted epoxy layers do not contribute to the strength and load-carrying capacity of the laminated tubes. The epoxy layers are modeled by the conventional S4R shell element and initially they were tied to the composite layers. Surface-to-surface interaction is used in the tie connection before the damage of the epoxy layers has occurred.

Two approaches to the modelling of yield in polymers (like epoxies) can be utilized: the use of non-linear viscoelasticity; and the direct application of metal plasticity (Ward and Sweeney^[43]). In the present study, the epoxy material is modeled as an isotropic elastic-plastic material^[44] using the in-built material model for metal plasticity in Abaqus when taking into account the effect of the hydrostatic stress. Table 5 lists the features of the selected material model (available in Abaqus material library)

FIGURE 4 Axial displacements of the adhesive epoxy layers: C1–C6 layers marked from inside out; Model AP-M1, $V_0 = 10$ m/s, $G = 49$ kg, $t = 0.002$ s [Color figure can be viewed at wileyonlinelibrary.com]

used to model the epoxy resin interface layer between composite laminae.

A simple ductile damage initiation criterion is used based on the critical strain in conjunction with the material triaxiality, η , while an energy criterion is adopted for damage evolution. After the full damage of the epoxy layers has occurred, the composite layers can interact with each other according to general contact behavior.

The fracture energy per unit area of the epoxy resin ($G_{f,\text{epoxy}}$) can be calculated as:

$$G_{f,\text{epoxy}} = \int_{\epsilon_0^{pl}}^{\epsilon_f^{pl}} L^c \sigma_y d\epsilon^{pl} = \int_0^{u_f^{pl}} \sigma_y du^{pl} \quad (1)$$

where L^c is the characteristic length of the shell elements, ϵ_0^{pl} and ϵ_f^{pl} are the initial and final plastic strains, and u_f^{pl}

FIGURE 5 Displacements magnitudes of the adhesive epoxy layers: C1–C6 layers marked from inside out; Model AP-M1, $V_0 = 10 \text{ m/s}$, $G = 49 \text{ kg}$, $t = 0.002 \text{ s}$ [Color figure can be viewed at wileyonlinelibrary.com]

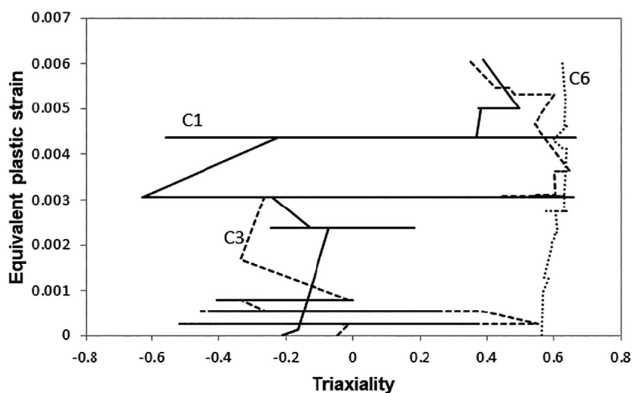
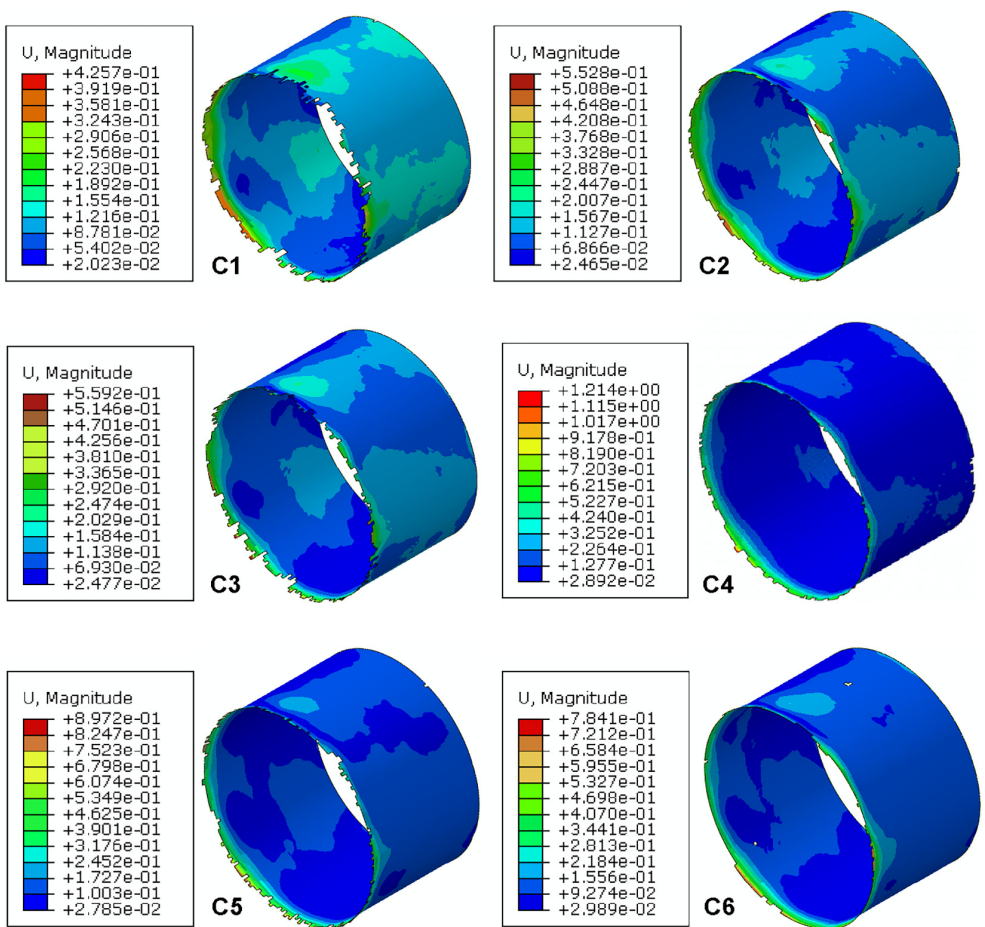


FIGURE 6 Equivalent plastic strains histories until damage initiation of layers C1, C3 and C6 of model AP-M1 - Arbitrary elements in the three epoxy layers

is the corresponding final displacement. In the case of a linear law for the damage evolution used here:

$$G_{f,\text{epoxy}} = L^c \left(\varepsilon_f^{pl} - \varepsilon_0^{pl} \right) \sigma(D=0)/2. \quad (2)$$

A typical stress-strain characteristic of the adhesive material is shown in Figure 3. The elastic modulus

$E = 3.6 \text{ GPa}$, Poisson ratio $\nu = 0.37$, the yield stress is $\sigma_Y = 36 \text{ MPa}$ and $\sigma(D=0) = 50 \text{ MPa}$ is the stress at the critical plastic strain at damage initiation. The density of the epoxy material used in the current FE models is $\rho = 1160 \text{ kg/m}^3$.^[44]

Besides the more straightforward implementation of the present interface modelling technique compared to other element based cohesive zone models (those using continuum elements), the present technique has a minimal effect on the time increment since the thickness of S4R interface layers will not affect the time increment in contrast to the continuum interface elements.

3 | VALIDATION OF THE PROPOSED MODEL

The FE model described in Section 2 was validated against the dynamic test results of the present authors.^[16] The test data used for the validation are summarized in Table 6. The selected loading parameters correspond to nearly equal initial kinetic energies applied to the tubes but having different initial velocities. The mesh is uniform with an average side length of the elements of 0.75 mm in all models.

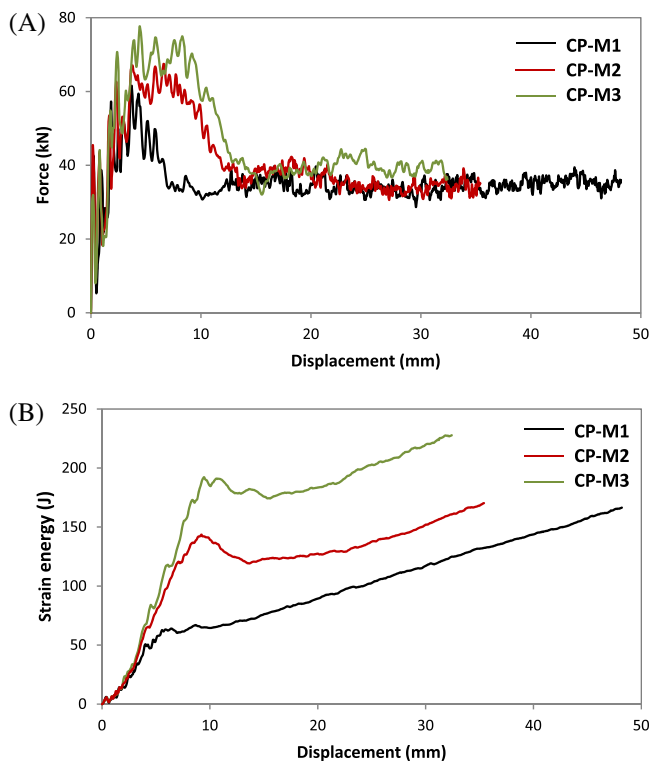


FIGURE 7 Responses of FE models of cross-ply tubes with different number of adhesive layers, CP-M1, CP-M2 and CP-M3, $V_0 = 10 \text{ m/s}$, $G = 49 \text{ kg}$; (A) Force-displacement histories; (B) Strain energy histories [Color figure can be viewed at wileyonlinelibrary.com]

The appearance of buckling modes in the components of the laminated tubes is demonstrated by the non-uniform displacements of the epoxy adhesive layers in the angle-ply model AP-M1 presented, as an example, in Figures 4 and 5 at $t = 0.002 \text{ s}$. The different axial (Figure 4) and combined displacement magnitudes (Figures 5) clearly illustrates the source of a more complex stress-state in the adhesion surfaces, which is difficult to be handled by the definition of critical normal and shear stress, displacement or strain only.

Under axial compression, the adhesive layers undergo a path-dependent deformation history which can start from compression in the axial direction followed by tension in the circumferential direction. The different strain-triaxiality histories of some arbitrary elements with the same y - and z -coordinates in epoxy layers C1, C3, and C6 are shown in Figure 6. The initial negative triaxiality in layers C1 and C3 corresponds to an initial dominant compression of these layers, which are closer to the inner surface of the laminated tube. On the other hand, the outermost epoxy layer, C6, undergoes only tensile deformation. Despite different strain histories, however, damage of the epoxy layers initiates in the tensile mode but with slightly different triaxiality. For plane stress

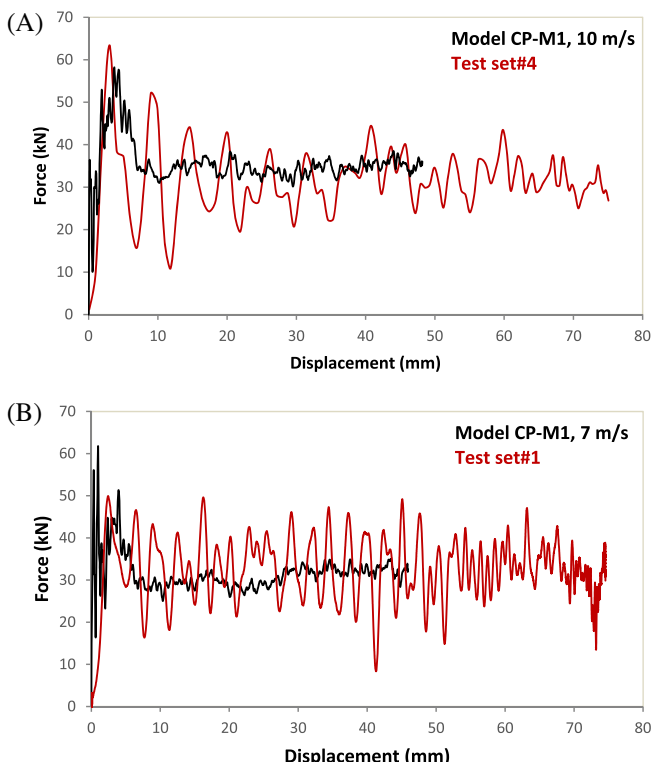


FIGURE 8 Comparison between the simulation and test results for cross-ply tubes; (A) $V_0 = 10 \text{ m/s}$, $G = 49 \text{ kg}$ (set#4, Table 6); (B) $V_0 = 7 \text{ m/s}$, $G = 100 \text{ kg}$ (set#1, Table 6) [Color figure can be viewed at wileyonlinelibrary.com]

conditions, $\eta = 1/3$ corresponds to uniaxial tension while $\eta = 2/3$ corresponds to equi-biaxial tension^[45] so that the obtained triaxiality values between $\eta = 0.344$ and 0.625 indicate stress states between uniaxial and equi-biaxial tension. The critical plastic strain of 0.006 was used together with $\eta = 1/3$ in all FE models assuming that the dependence of the strain of epoxy resin on the triaxiality is weak for $\eta > 1/3$.^[46]

3.1 | Cross-ply FE models

It was established through the simulation analysis that the cross-section delamination plays an important role in the prediction of the force-displacement history, particularly in the range of relatively small axial displacements. Three models of the cross-ply tubes were developed when assuming different numbers of adhesive layers modelling the delamination (Table 3). The essential difference between models CP-M1 and CP-M3 is that the 90° layers in CP-M1 are modelled as double layers with inserted epoxy layers to model delamination within the 0.6 mm thick layers. Model CP-3 contains single 0.6 mm thick layers between the 0° layers. In model CP-M2, the 90°

FIGURE 9 Comparison between the damaged tubes; (A),(B) FE simulation, model CP-M1, $V_0 = 7 \text{ m/s}$, $G = 100 \text{ kg}$; (C) drop test, set#1 [Color figure can be viewed at wileyonlinelibrary.com]

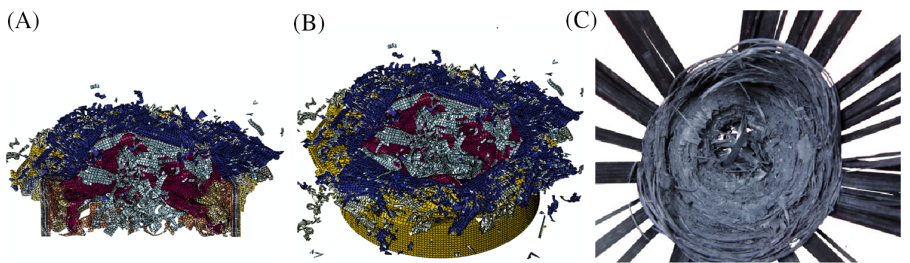
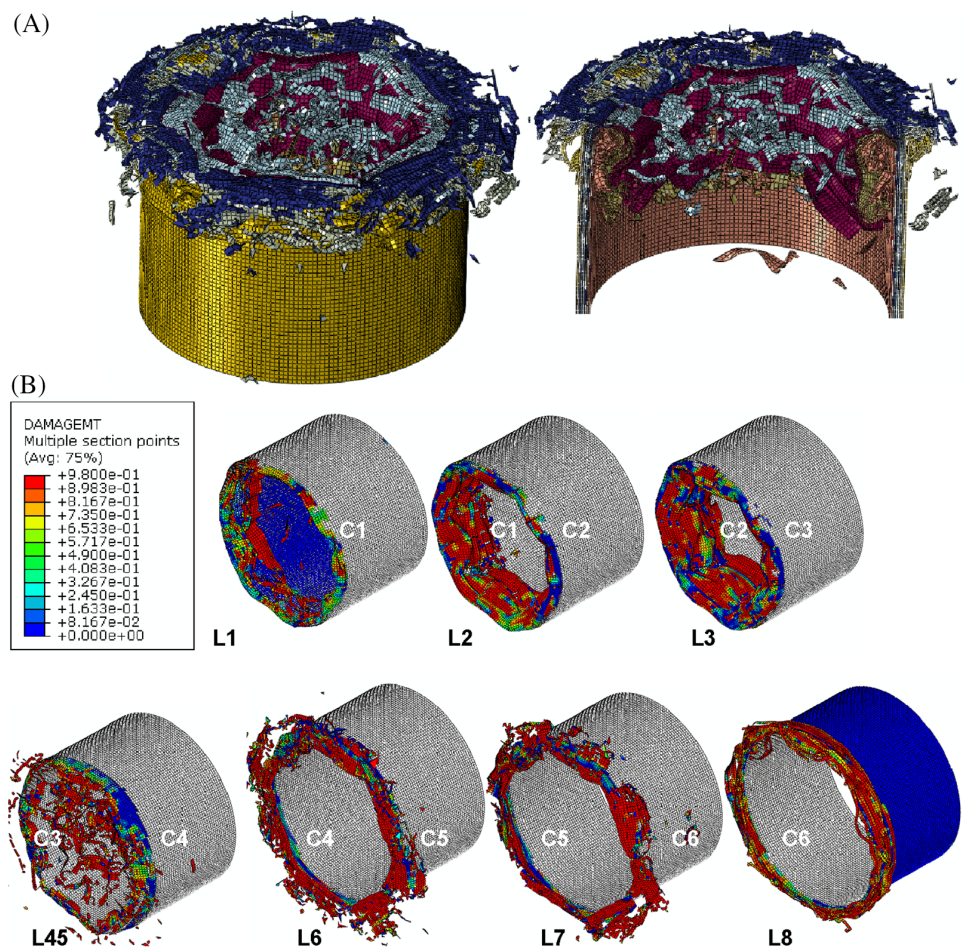


FIGURE 10 Damage and delamination of the cross-ply model CP-M1, $V_0 = 10 \text{ m/s}$, $G = 49 \text{ kg}$, $t = 0.0032 \text{ s}$; (A) Damage and deformation of the tube model; (B) Composite layers and surrounding adhesive layers: composite layers L1–L8 (see Table 3) and adhesive (resin) layers C1–C6 are marked from insight out [Color figure can be viewed at wileyonlinelibrary.com]



layers are modelled with double plies, therefore they cannot delaminate before damaging of either ply.

A comparison between the force-displacement histories resulting from the three models is shown in Figure 7(A). The 90° layers break due to fiber tension/compression but obviously, they cannot damage easily when using relatively thick layers in model CP-M3 due to the inability of delamination. The intact material of the tube invokes lateral inertia effects, which results in a significant increase of the crushing force keeping a high value at relatively large axial displacements (approximately 10 mm, Figure 7(A)). By contrast, the possibility of delamination within the 90° layers in CP-M1 allows the development of larger displacements and strains in the circumferential direction after delamination. The lateral inertia effects become

much smaller leading to a lower peak load which drops quickly at a crash distance of about 5 mm. The approximation of the 90° layers by double layers in CP-M2 affects slightly the maximum load but it has also an effect on the mean load when comparing this model to CP-M3. It is shown in Figure 7(B) that the stored strain energy in model CP-M3 during the peak formation increases more rapidly in comparison with the other two models due to the reduced ability of delamination.

The results in Figure 7(A) indicate that model CP-M1 gives more realistic predictions. This model is further used for validation purposes for impacts with different initial velocities. The force-displacement histories obtained numerically using model CP-M1 and as a result of the drop tests are compared in Figure 8(A),(B) for the

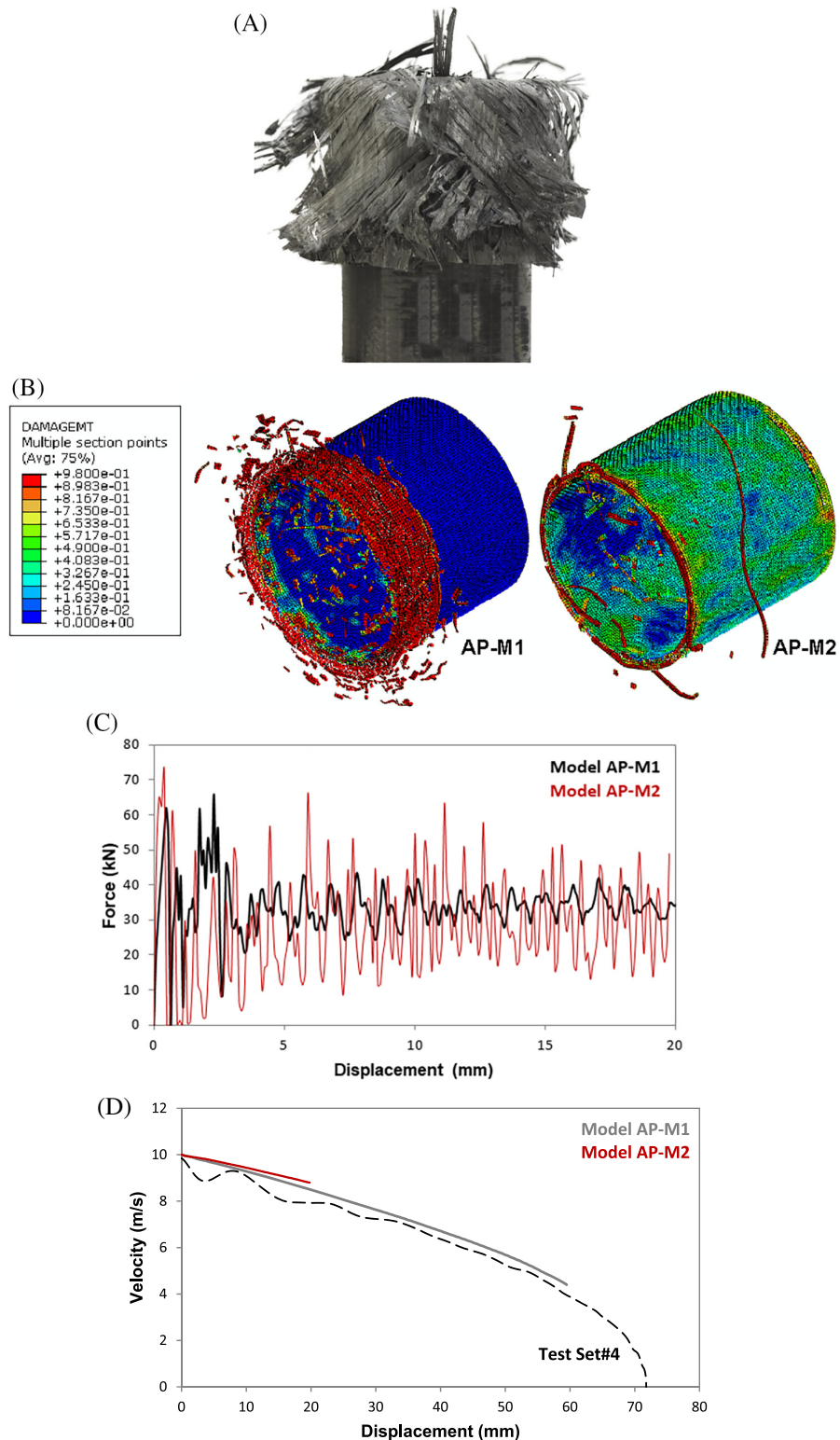


FIGURE 11 Comparison between the response of cross-ply models AP-M1 and AP-M2, element size 0.75 mm, $V_0 = 10 \text{ m/s}$, $G = 49 \text{ kg}$, $t = 0.002 \text{ s}$; (A) Final deformed shape of the tested tube^[16]; (B) Deformed shapes obtained numerically; (C) Force-displacement characteristics; (D) Velocity attenuation; the dashed line presents the experimental velocity-displacement curve [Color figure can be viewed at wileyonlinelibrary.com]

same initial kinetic energy but applied at different initial velocities. A reasonable agreement is observed although higher magnitude oscillations occur during the experimental tests. The observed differences between the force-displacement curves in Figure 7(A) and drop test result in Figure 8(A) indicate that a sufficient number of

delamination surfaces has to be used in the FE model in order to obtain accurate force-displacement predictions.

The deformed shapes predicted by model CP-M1 for an impact at $V_0 = 7 \text{ m/s}$ with $G = 100 \text{ kg}$ and the tested cross-ply tube, set#1, are shown in Figure 9(A)–(C), respectively. It is evident that the damage is well

FIGURE 12 Damage and delamination of the angle-ply model AP-M1, $V_0 = 10$ m/s, $G = 49$ kg, $t = 0.0048$ s; (A) Damage and deformation of the tube model; (B) Composite layers with neighboring adhesive layers: L1–L7 (see Table 3) and adhesive (resin) layers C1–C6 are marked from insight out [Color figure can be viewed at wileyonlinelibrary.com]

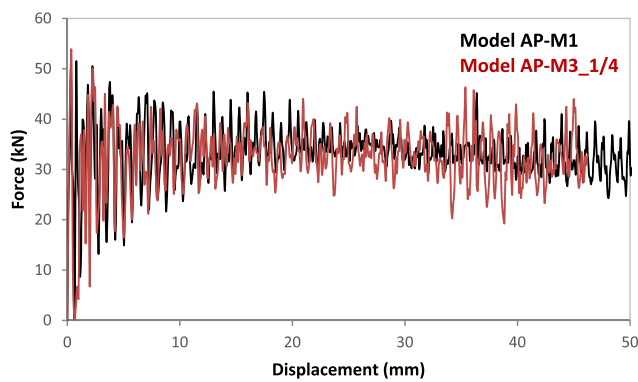
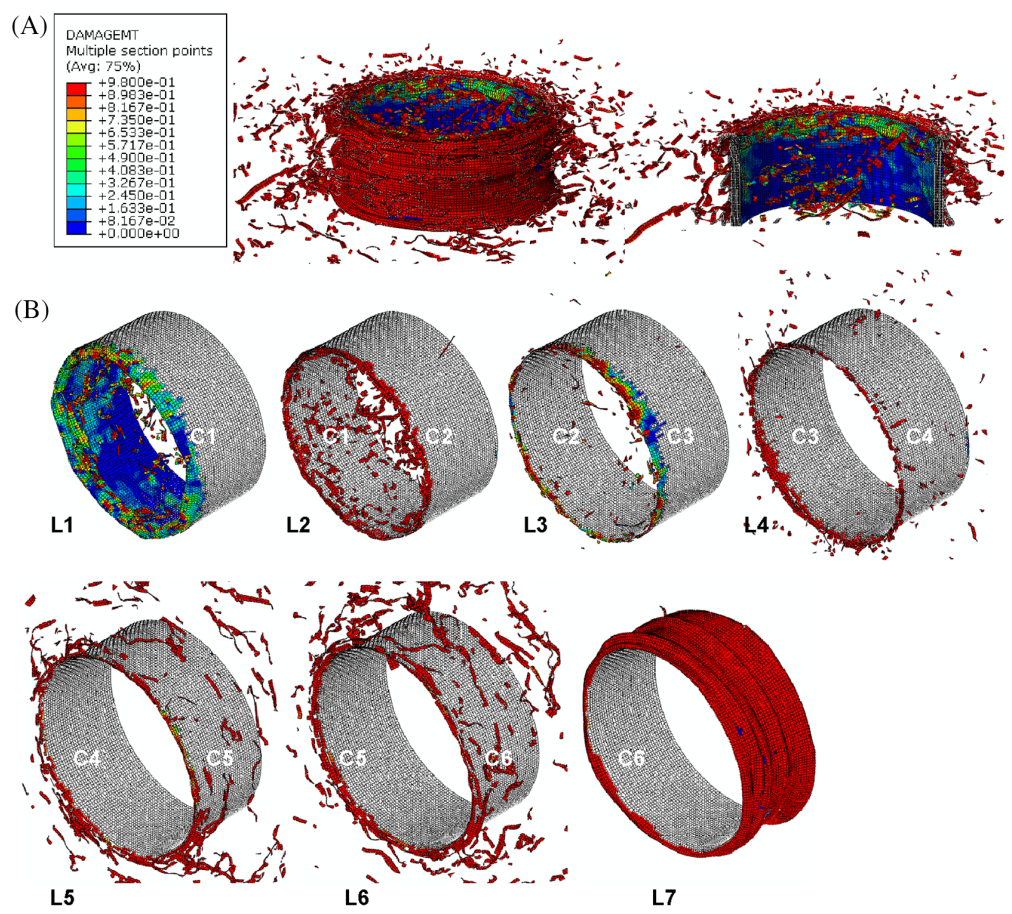


FIGURE 13 Effect of using symmetry conditions for cross-ply tubes, comparison between force-displacement histories for models AP-M1 and AP-M3_1/4, $V_0 = 10$ m/s, $G = 49$ kg [Color figure can be viewed at wileyonlinelibrary.com]

represented by the FE model except for the damage of the outermost composite layer of the cross-ply tube (0° layer). A specific damage mode of the one-side constrained layer occurs during the drop test. The outermost 0° layer splits into pieces along the fiber direction due to the matrix failure in the transverse direction and delaminates from the adjacent layer (Figure 9(C)). This mode is

an intra-laminar damage mode resulting from the fiber-matrix delamination,^[47] which cannot be captured by the algorithm of element deletion used together with Hashin 2D damage model. The internal 0° layer (placed in the middle of the cross-section) fails in either a bending mode or fiber kinking mode, which is represented by the model. Despite the inaccurate prediction of the damage mode of the outermost 0° layer, the overall stiffness of the composite layers is approximated with sufficient accuracy, which is confirmed by the agreement between the experimental and numerical force-displacement histories in Figure 8. The initial force drop, as well as the average force, agrees well, even considering the large fluctuations of the force. It should be noted that the experimental force-displacement signal was high frequency filtered.

The ability of the proposed approach to model delamination by the degradation of the connecting resin layers is demonstrated in Figure 10 where the deformed shapes and damage of the cross-ply model CP-M1 for an impact with $V_0 = 10$ m/s and $G = 49$ kg at $t = 0.0032$ s are shown. The deformation and damage of the individual composite layers (L-layers) surrounded by the adhesive layers (C-layers) (presented from the inside out of the tube) are shown in Figure 10(B). The fringe levels of

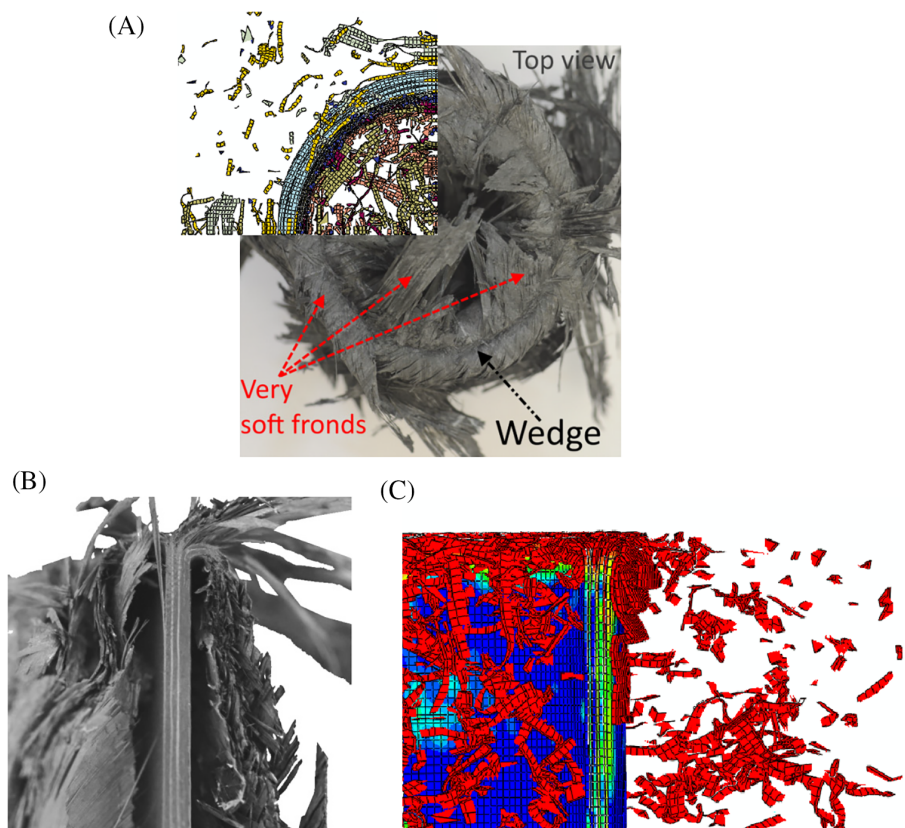


FIGURE 14 Deformed shape and damage of an angle-ply tube; (A) Top view, $V_0 = 5 \text{ m/s}$, $G = 196 \text{ kg}$ (set#3); (B) Drop test, set#1; (C) model AP-M3_1/4, $V_0 = 7 \text{ m/s}$, $G = 100 \text{ kg}$ [Color figure can be viewed at wileyonlinelibrary.com]

damage parameter DAMAGEMT refer to the composite layers and the resin layers appear in gray color as this variable is not defined for them. The deleted parts of the C-layers represent the area where delamination has occurred. It is clear that delamination develops prior to damage of the composite layers and it propagates across 3–4 elements in the direction of loading, or 2.25–3 mm, which is comparable with the tube thickness. The same response was observed from the tests where the delamination developed first followed by damage of the composite layers. Similar to the tests, layers L1, L2, L3 and L45 deform predominantly inward while layers L6, L7, and L8 deform outward. Fiber breakage in tension/compression develops in L2, L3, L6, and L7 representing 90° material orientation.

3.2 | Angle-ply FE models

The validation of the angle-ply model is presented in the following examples. Similar to the models of the cross-ply tubes, the effect of the number of adhesive layers modeling the delamination is analyzed when comparing the responses of models AP-M1 and AP-M2 (see Table 3). Six adhesive layers are used in model AP-M1 while only two adhesive layers are used in model AP-M2. In the latter model, thicker multiple plies with different fiber

orientations are used. The deformed shapes and damage predicted by these two models are compared in Figure 11(B) for an impact with $V_0 = 10 \text{ m/s}$, $G = 49 \text{ kg}$ at $t = 0.002 \text{ s}$. Somewhat unrealistic deformed shape is predicted by model AP-M2 when comparing it with the tested specimen in Figure 11(A). The thicker composite layers of this model possess higher bending rigidity in comparison with the relatively thin delaminated layers in the tests so that they are unable to reproduce bending accurately. The majority of the elements of AP-M2 model are damaged in compression/tension and the damaged portion of the tube is deleted. The deformed shape of AP-M1 is closer to the shape observed during the drop tests due to the better modelling of bending after the delamination of the thinner composite layers. The force-displacement histories corresponding to the two models are shown in Figure 11(C) where the highly oscillating curve corresponds to model AP-M2. This curve defines an average force of 27.98 kN, which is considerably lower than the average force of 32.5 kN predicted by the AP-M1 model. The velocity-displacement curves in Figure 11(D) indicate that the initial impact velocity is more rapidly attenuated by model AP-M1 thus representing more accurate the test results. Indeed, this velocity-displacement behavior corresponds to the higher average force predicted by model AP-M1. For this reason, the further analysis of the

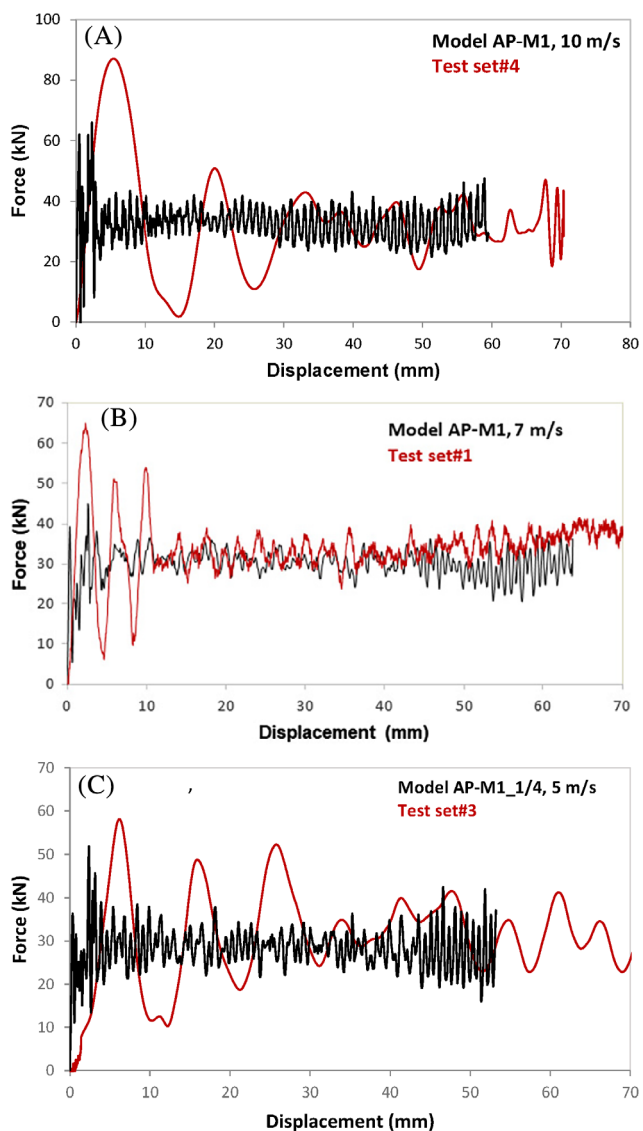


FIGURE 15 Comparison between the simulation and test results for angle-ply tubes; (A) $V_0 = 10 \text{ m/s}$, $G = 49 \text{ kg}$ (set#4); (B) $V_0 = 7 \text{ m/s}$, $G = 100 \text{ kg}$ (set#1); (C) $V_0 = 5 \text{ m/s}$, $G = 196 \text{ kg}$ (set#3) [Color figure can be viewed at wileyonlinelibrary.com]

angle-ply tubes is carried out when using the cross-section model with six adhesive layers.

The deformed shapes and damage of the angle-ply model AP-M1 for an impact with $V_0 = 10 \text{ m/s}$ and $G = 49 \text{ kg}$ at $t = 0.0032 \text{ s}$ is shown in Figure 12. The deformation and damage of the individual composite layers with adjacent adhesive layers show that the delamination has propagated no further than three elements (2.25 mm), which is again comparable with the tube thickness as it was observed in the crushing tests.^[16]

In order to reduce the computational time, one-quarter of the angle-ply tube was modeled (Figure 1(B)) although the model does not strictly satisfy the symmetry conditions

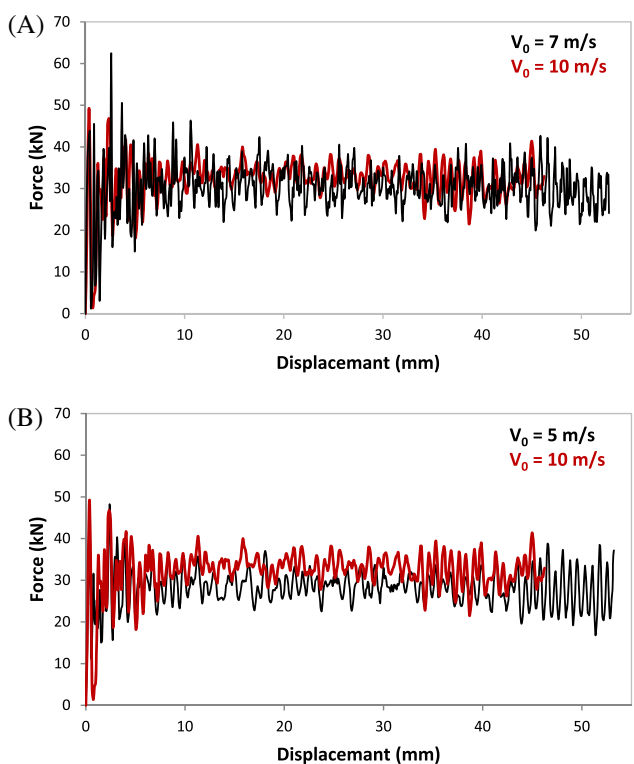


FIGURE 16 Influence of the impact velocity, model AP-M3_1/4; (A) Impacts with $V_0 = 10 \text{ m/s}$, $G = 49 \text{ kg}$ (set#4) and $V_0 = 7 \text{ m/s}$, $G = 100 \text{ kg}$ (set#1); (B) Impacts with $V_0 = 10 \text{ m/s}$, $G = 49 \text{ kg}$ and $V_0 = 5 \text{ m/s}$, $G = 186 \text{ kg}$ (set#3) [Color figure can be viewed at wileyonlinelibrary.com]

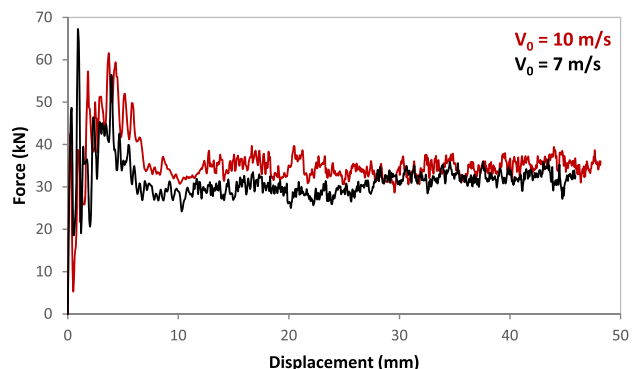


FIGURE 17 Influence of the impact velocity, model CP-M1, impacts with $V_0 = 10 \text{ m/s}$, $G = 49 \text{ kg}$ (set#4) and $V_0 = 7 \text{ m/s}$, $G = 100 \text{ kg}$ (set#1) [Color figure can be viewed at wileyonlinelibrary.com]

due to the damage along the planes of symmetry. Nevertheless, overall, satisfactory results were obtained in terms of force-displacement characteristics and damage modes. The force-displacement curves corresponding to models AP-M1 and AP-M3_1/4 for an impact with $V_0 = 10 \text{ m/s}$ and $G = 49 \text{ kg}$ are compared in Figure 13(A). A small difference between the predicted average forces is observed

when the value predicted by the AP-M3_1/4 model is about 2.5% lower than that of model AP-M1.

Model AP-M3_1/4 was further used to model the impacts with $V_0 = 7 \text{ m/s}$, $G = 49 \text{ kg}$ and $V_0 = 5 \text{ m/s}$, $G = 196 \text{ kg}$. The numerically obtained deformed shapes and damage of the cross-ply tubes are compared with the test results in Figure 14 where an agreement between the two sets of results is observed. Overall, the results in Figures 13 and 14 show that the six adhesive layers model can adequately predict the deformation and damage of angle-ply tubes.

Comparisons between the force-displacement curves recorded during the drop-tests and numerically obtained curves are shown in Figures 15(A)–(C). It is observed that the EF model underestimates the initial peak load but it predicts very well the average forces for the three examined cases. Fluctuations with larger magnitudes occur during the tests, particularly for the impact with $V_0 = 5 \text{ m/s}$ where the excessive high-frequency filtering has caused an unphysical shift of the peak load toward the larger axial displacements.

3.3 | Influence of the impact velocity

The developed FE model with resin layers modelling the adhesion between the composite ones are used to analyze the influence of the impact velocity on the force-displacement histories and thus on the specific energy absorption of laminated tubes when applying impacts with equal initial kinetic energies but different impact velocities and consequently different striking masses. The tube responses to impacts with initial velocities of 5, 7, and 10 m/s are simulated with impact masses of 196, 100, and 49 kg, respectively. These loading parameters are close to the test loading parameters given in Table 6.

The sensitivity to the loading rate of the angle-ply tubes is examined by using AP-M1_1/4 model. The results of the numerical simulations are shown in Figure 16(A),(B). No significant difference between the force-displacement curves is observed. Since no strain rate effect of the constituent materials is taken into account, only the lateral inertia can cause a force increase by delaying the layers' delamination. However, the range of velocity variation is relatively small in order to observe a significant effect.

The sensitivity to the loading rate of the cross-ply tubes is examined by using the model CP-M1 and the results of the numerical simulations are presented in Figure 17. A small inertia effect is observed in this lay-up configuration only during the early stage of deformation. Overall, the observed dynamic effect in the examined cross-ply and angle-ply laminated tubes is small which is

also due to the small difference between the initial impact velocities. No definite effect of the loading rate was also observed for the tested CFRP tubes in.^[16]

4 | CONCLUSIONS

The dynamic axial crushing response of circular tubes made of unidirectional carbon fiber-epoxy composite was investigated numerically in the present study using Abaqus/Explicit code. A new approach to the delamination of CFRP tubes under axial low velocity impact is proposed so to replace the commonly used surface-based cohesive interaction model. The developed approach uses the idea of the adhesive epoxy layers capable of damage. The epoxy layers are modelled by conventional shell element tied to the adjacent composite layers. The proposed approach eliminates the phenomenon of premature delamination caused by the development of buckling models with different magnitudes in the individual composite layers (see Appendix 0). The use of conventional S4R shell elements to model both the composite and adhesive layers reduces significantly the computational time in comparison with the time for delamination modelling based on cohesive elements.

The developed approach to delamination was validated against low-velocity drop tests performed by the authors on angle-ply and cross-ply tubes at several impact velocities.^[16] In this study, attention is paid to the influence of the number of adhesive layers modelling the delamination on the accuracy of the predicted force-displacement characteristics. Good agreement was achieved when using a sufficient number of interfaces between the composite layers to allow delamination similar to the one observed in the tests. The brief discussion on the influence of the loading rate on the response of some laminated tubes indicates that the proposed modelling technique can yield the same conclusions obtained experimentally.

The proposed approach to delamination can be applied to axially loaded laminated structural components with multiple buckling modes of the individual layers.

ACKNOWLEDGEMENTS

The financial support of the Brazilian funding agency CNPq (Project 401092/2014-3) for this research is gratefully acknowledged. Dora Karagiozova acknowledges the partial support by Grant No BG05M2OP001-1.001-0003-C01 financed by the Science and Education for Smart Growth Operational Program (2014-2020) and co-financed by the European Union through the European Structural and Investment funds.

ORCID

Marcilio Alves  <https://orcid.org/0000-0002-0285-8276>

REFERENCES

- [1] A. G. Mamalis, D. E. Manolakos, G. A. Demosthenous, M. B. Ioannidis, *Thin-Walled Struct.* **1996**, 24, 335. [https://doi.org/10.1016/0263-8231\(95\)00042-9](https://doi.org/10.1016/0263-8231(95)00042-9).
- [2] M. Morthorst, P. Horst, *J. Strain Anal. Eng. Des.* **2004**, 39, 411. <https://doi.org/10.1243/0309324041896443>.
- [3] R. Bogenfeld, J. Kreikemeier, T. Wille, *Eng. Fail. Anal.* **2018**, 86, 72. <https://doi.org/10.1016/j.englfailanal.2017.12.019>.
- [4] Y. Shi, T. Swait, C. Soutis, *Compos. Struct.* **2012**, 94, 2902. <https://doi.org/10.1016/j.compstruct.2012.03.039>.
- [5] D. Feng, F. Aymerich, *Compos. Struct.* **2014**, 108, 161. <https://doi.org/10.1016/j.compstruct.2013.09.004>.
- [6] P. F. Liu, B. B. Liao, L. Y. Jia, X. Q. Peng, *Compos. Struct.* **2016**, 149, 408. <https://doi.org/10.1016/j.compstruct.2016.04.012>.
- [7] A. Riccio, A. De Luca, G. Di Felice, F. Caputo, *Compos. Part B: Eng.* **2014**, 66, 340. <https://doi.org/10.1016/j.compositesb.2014.05.024>.
- [8] Y. Wang, S. Zhu, J. Qi, J. Xiao, *Polym. Polym. Compos.* **2014**, 22, 73. <https://doi.org/10.1177/096739111402200111>.
- [9] M. V. Donadon, L. Iannucci, B. G. Falzon, J. M. Hodgkinson, S. F. M. de Almeida, *Comput. Struct.* **2008**, 86, 1232. <https://doi.org/10.1016/j.compstruc.2007.11.004>.
- [10] S. M. R. Khalili, M. Sorough, A. Davar, O. Rahmani, *Compos. Struct.* **2011**, 93, 1363. <https://doi.org/10.1016/j.compstruct.2010.10.003>.
- [11] V. Tita, J. de Carvalho, D. Vandepitte, *Compos. Struct.* **2008**, 83, 413. <https://doi.org/10.1016/j.compstruct.2007.06.003>.
- [12] A. Sellitto, S. Saputo, F. Di Caprio, A. Riccio, A. Russo, V. Acanfora, *Appl. Sci.* **2019**, 9, 2372. <https://doi.org/10.3390/app912372>.
- [13] F. Caputo, F. Di Gennaro, G. Lamanna, A. Lefons, A. Riccio, *Key Eng. Mater.* **2013**, 569-570, 111. <https://doi.org/10.4028/www.scientific.net/KEM.569-570.111>.
- [14] Y. Zhang, L. Sun, L. Li, H. Xiao, Y. Wang, *Polym. Compos.* **2020**, 41, 2673. <https://doi.org/10.1002/pc.25566>.
- [15] M. Sorough, K. M. Fard, M. Shahrvani, *Latin Am. J. Solids Struct.* **2018**, 15(6), e90. <https://doi.org/10.1590/1679-78254609>.
- [16] P. B. Ataabadi, D. Karagiozova, M. Alves, *Int. J. Impact Eng.* **2019**, 131, 174. <https://doi.org/10.1016/j.ijimpeng.2019.03.006>.
- [17] G. Zhu, G. Sun, H. Yu, S. Li, Q. Li, *Int. J. Mech. Sci.* **2018**, 135, 458. <https://doi.org/10.1016/j.ijmecsci.2017.11.017>.
- [18] X. Zhao, G. Zhu, C. Zhou, Q. Yu, *Compos. Struct.* **2019**, 222, 110920. <https://doi.org/10.1016/j.compstruct.2019.110920>.
- [19] A. G. Mamalis, D. E. Manolakos, M. B. Ioannidis, D. P. Papapostolou, *Compos. Struct.* **2006**, 74, 213. <https://doi.org/10.1016/j.compstruct.2005.04.006>.
- [20] J. Huang, X. Wang, *Compos. Struct.* **2009**, 91, 222. <https://doi.org/10.1016/j.compstruct.2009.05.006>.
- [21] C. McGregor, R. Vaziri, X. Xiao, *Int. J. Impact Eng.* **2010**, 37, 662. <https://doi.org/10.1016/j.ijimpeng.2009.09.005>.
- [22] D. Siromani, J. Awerbuch, T. M. Tan, *Compos. Part B: Eng.* **2014**, 64, 50. <https://doi.org/10.1016/j.compositesb.2014.04.008>.
- [23] C. McGregor, N. Zobeiry, R. Vaziri, A. Poursartip, X. Xiao, *Compos. Part A: Appl. Sci. Manuf.* **2017**, 95, 208. <https://doi.org/10.1016/j.compositesa.2017.01.012>.
- [24] C. Reuter, K. H. Sauerland, T. Tröster, *Compos. Struct.* **2017**, 174, 33. <https://doi.org/10.1016/j.compstruct.2017.04.052>.
- [25] M. Dlugosch, J. Fritsch, D. Lukaszewicz, S. Hiermaier, *Compos. Struct.* **2017**, 174, 338. <https://doi.org/10.1016/j.compstruct.2017.04.077>.
- [26] Dassault Systèmes Simulia, Abaqus 6.14. Analysis User's Guide, (2014). <https://doi.org/10.1017/CBO9781107415324.004>.
- [27] S. Palanivelu, W. Van Paepgem, J. Degrieck, D. Kakogiannis, J. Van Ackeren, D. Van Hemelrijck, J. Wastiels, J. Vantomme, *Polym. Test.* **2010**, 29, 729. <https://doi.org/10.1016/j.polymertesting.2010.05.010>.
- [28] S. Patel, V. R. Vusa, C. Guedes Soares, *Int. J. Mech. Sci.* **2019**, 156, 221. <https://doi.org/10.1016/j.ijmecsci.2019.03.038>.
- [29] V. S. Sokolinsky, K. C. Indermuehle, J. A. Hurtado, *Compos. Part A: Appl. Sci. Manuf.* **2011**, 42, 1119. <https://doi.org/10.1016/j.compositesa.2011.04.017>.
- [30] F. L. Matthews, G. A. O. Davies, D. Hitchings, C. Soutis, Composites and finite element analysis. in: *Finite Elem. Model. Compos. Mater. Struct.*, Elsevier, **2000**, p. 71. <https://doi.org/10.1533/9781855738928.3.69>.
- [31] L. N. S. Chiu, B. G. Falzon, R. Boman, B. Chen, W. Yan, *Compos. Struct.* **2015**, 131, 215. <https://doi.org/10.1016/j.compstruct.2015.05.008>.
- [32] L. N. S. Chiu, B. G. Falzon, B. Chen, W. Yan, *Compos. Struct.* **2016**, 147, 65. <https://doi.org/10.1016/j.compstruct.2016.03.028>.
- [33] W. Tan, B. G. Falzon, *Compos. Sci. Technol.* **2016**, 134, 57. <https://doi.org/10.1016/j.compscitech.2016.07.015>.
- [34] W. Tan, B. G. Falzon, M. Price, *Int. J. Crashworthiness* **2015**, 20, 60. <https://doi.org/10.1080/13588265.2014.972122>.
- [35] P. B. Ataabadi, D. Karagiozova, M. H. Shaterzadeh, M. Alves, *Compos. Struct.* **2020**, 245, 112382. <https://doi.org/10.1016/j.compstruct.2020.112382>.
- [36] Z. Hashin, *J. Appl. Mech.* **1980**, 47, 329. <https://doi.org/10.1115/1.3153664>.
- [37] <https://www.3ds.com/products-services/simulia/services-support/support/documentation/>
- [38] S. Boria, G. Belingardi, D. Fiumarella, A. Scatina, *Compos. Struct.* **2019**, 226, 111241. <https://doi.org/10.1016/j.compstruct.2019.111241>.
- [39] Y. Shi, C. Pinna, C. Soutis, Low-velocity impact of composite laminates: Damage evolution. In: *Dynamic Deformation, Damage and Fracture in Composite Materials and Structures*, Ed. Vadim V. Silberschmidt, pp. 117–146, Elsevier, Amsterdam. **2016**. <https://doi.org/10.1016/b978-0-08-100080-9.00005-1>.
- [40] C. Zhang, E. A. Duodu, J. Gu, *Compos. Struct.* **2017**, 173, 219. <https://doi.org/10.1016/J.COMPSTRUCT.2017.04.017>.
- [41] J. Reeder, K. Song, P. Chunchu, D. Ambur, Postbuckling and Growth of Delaminations in Composite Plates Subjected to Axial Compression, in: 43rd AIAA/ASME/ASCE/AHS/ASC Structural Dynamics Material Conference., American Institute of Aeronautics and Astronautics, Reston, Virigina, **2002**. <https://doi.org/10.2514/6.2002-1746>.
- [42] E. V. González, P. Maimí, E. Martín-Santos, A. Soto, P. Cruz, F. Martín de la Escalera, J. R. Sainz de Aja, *Int. J. Solids Struct.* **2018**, 144–145, 230. <https://doi.org/10.1016/j.ijsolstr.2018.05.005>.
- [43] I. M. Ward, J. Sweeney, *Mechanical Properties of Solid Polymers*, John Wiley & Sons, Ltd, Chichester, UK **2012**. <https://doi.org/10.1002/9781119967125>.

- [44] E. A. Nekliudova, A. S. Semenov, B. E. Melnikov, S. G. Semenov, *Mag. Civ. Eng.* **2014**, 47, 25. <https://doi.org/10.5862/MCE.47.3>.
- [45] M. Kõrgesaar, *Mar. Struct.* **2019**, 63, 45. <https://doi.org/10.1016/j.marstruc.2018.08.004>.
- [46] X.P. Morelle, F. Lani, M.A. Melchior, S. André, C. Bailly, T. Pardoen, The elasto-plasticity and fracture behaviour of the rtm6 structural epoxy and impact on the response of woven composites, in: *ECCM15-15th European Conference on Composites of Materials*, Venice, **2012**.
- [47] T. J. Vaughan, C. T. McCarthy, *Compos. Sci. Technol.* **2011**, 71, 388. <https://doi.org/10.1016/j.compscitech.2010.12.006>.
- [48] Z. Zou, S. R. Reid, S. Li, *J. Mech. Phys. Solids* **2003**, 51, 333. [https://doi.org/10.1016/S0022-5096\(02\)00075-3](https://doi.org/10.1016/S0022-5096(02)00075-3).

How to cite this article: Karagiozova D, Ataabadi PB, Alves M. Finite element modeling of CFRP composite tubes under low velocity axial impact. *Polymer Composites*. 2021;42:1543–1564. <https://doi.org/10.1002/pc.25923>

APPENDIX A: Validation of the material model parameters

Essential material and damage parameters used in the FE analysis were validated by the simulation of tensile

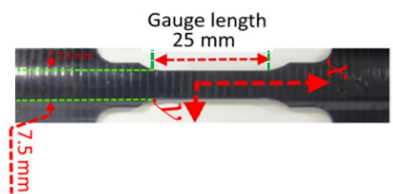


FIGURE A1 Geometry of the tensile specimen^[31] [Color figure can be viewed at wileyonlinelibrary.com]

tests on angle-ply and cross-ply specimens when using ABAQUS/Explicit. The tensile specimens were aligned with the longitudinal axis of the tested tubes and cut with a gauge length $L_{gauge} = 25$ mm and section width $L_{section} = 7.5$ mm (Figures A1, A2).

Due to the very small curvature of the tested specimens, flat FE models were built as shown in Figure A2. Shell elements S4R are used with composite cross-section. The ply compositions correspond to models AP-M1 (angle-ply) and CP-M1 (cross-ply) in Table 3; resin layers with a thickness of 0.02 mm are placed between the composite plies using tie connection as described in the main body of the paper. Material and damage parameters listed in Tables 2 and 4 are used in the simulations. The left boundary of the model was clamped and all degrees of freedom were constrained. The constant velocity of 20 mm/s was applied to the right end of the model to perform tension

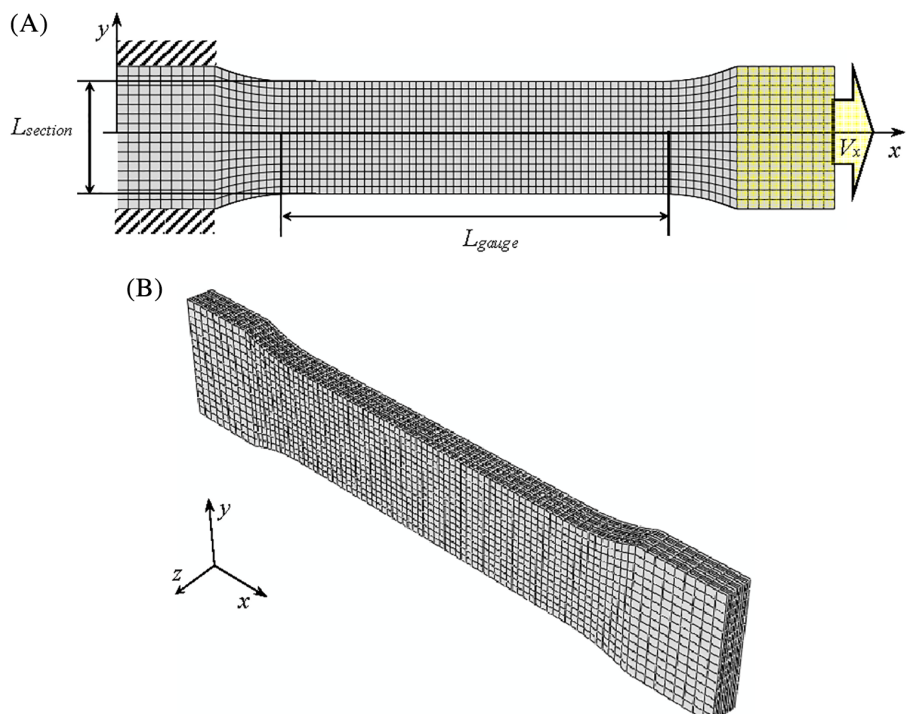


FIGURE A2 Geometry of the tensile specimen model. (A) Front view; (B) 3D view of the angle-ply model [Color figure can be viewed at wileyonlinelibrary.com]

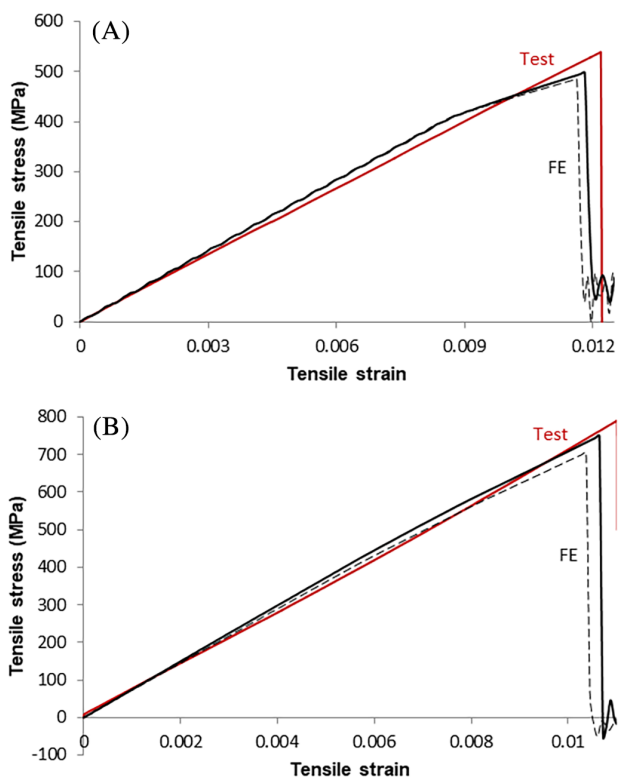


FIGURE A3 Comparison between the numerical and experimental tensile test results for average element size 0.75 mm (dashed line) and 0.5 mm (solid line); (A) Tensile testing on the angle-ply specimen; (B) Tensile testing on the cross-ply specimen [Color figure can be viewed at wileyonlinelibrary.com]

(Figure A2(A)). FE results obtained with velocities between 5 and 50 mm/s were nearly identical when using S4R elements of the same size.

Simulations with S4R elements with average side lengths of 0.5, 0.6, and 0.75 mm within the gauge area were performed to estimate the influence of the element size on the tensile stress and strain. Figure A3 shows comparisons between the experimental tensile test results and FE results using elements with side lengths of 0.5 and 0.75 mm. The results agree reasonably well while the FE results predict slightly lower values of the stresses and strains for both ply configurations. The agreement between the FE and test results improves when using smaller elements.

APPENDIX B: Mesh sensitivity analysis

Results from the mesh sensitivity analysis are shown in Figures B1–B3. The force-displacement histories obtained from the angle-ply model AP-M1 for an impact by a mass of 49 kg and initial velocity of 10 m/s meshed with S4R elements having average side lengths of 0.75, 1.0, and

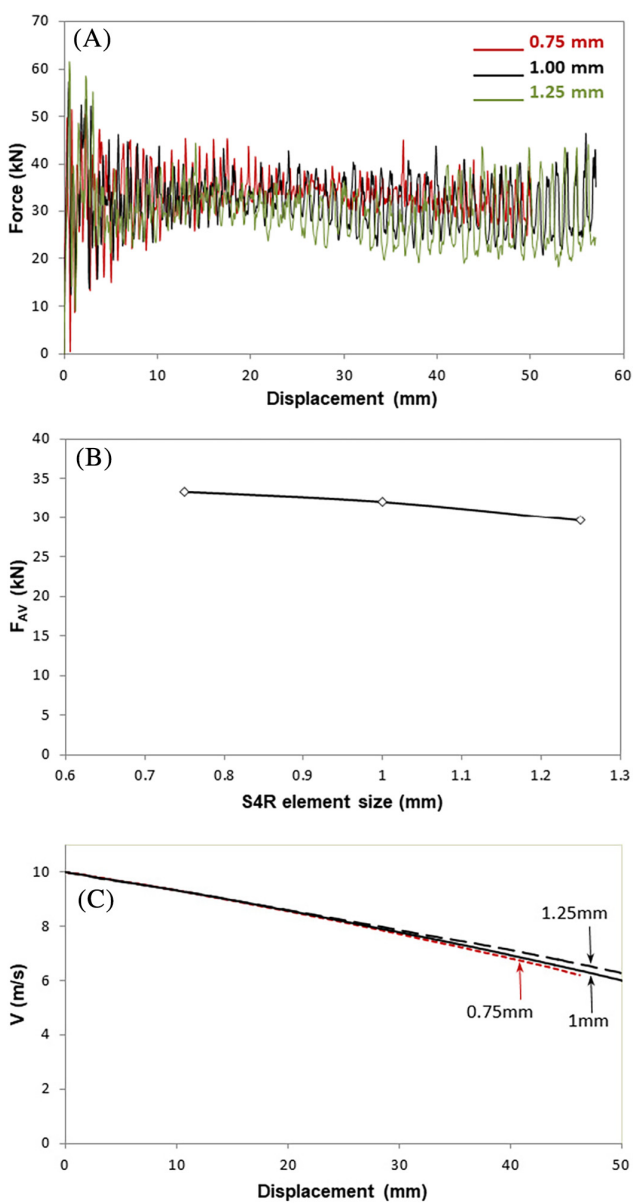


FIGURE B1 Mesh sensitivity of the model AP-M1, $L = 65$ mm, $V_0 = 10$ m/s, $G = 49$ kg; (A) Force-displacement histories for three element sizes; (B) Average forces; (C) Velocity attenuation [Color figure can be viewed at wileyonlinelibrary.com]

1.25 mm are compared in Figure B1(A) while the corresponding average forces are shown in Figure B1(B). The velocity attenuation histories due to the three models are shown in Figure B1(C). It is evident that differences resulting from the three mesh models exist but the difference reduces with decreasing the mesh size. It should be noted, however, that the decrease of the mesh size increases significantly the CPU time and further mesh refinement is impractical. A comparison between the deformed shapes of models with element size 0.75 and 1.25 mm are shown in Figure B2(A),(B), respectively at $t = 0.0028$ s. The mesh size effect causes only a marginal

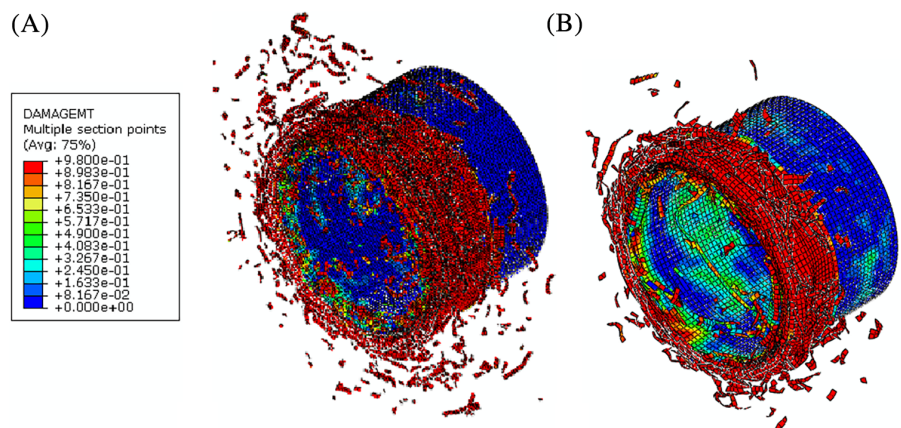


FIGURE B2 Deformed angle-ply tubes, model AP-M1, $V_0 = 10$ m/s, $G = 49$ kg, $t = 0.0028$ s; (A) Mesh size 0.75 mm, crush distance 25.34 mm; (B) Mesh size 1.25 mm, crush distance 25.46 mm [Color figure can be viewed at wileyonlinelibrary.com]

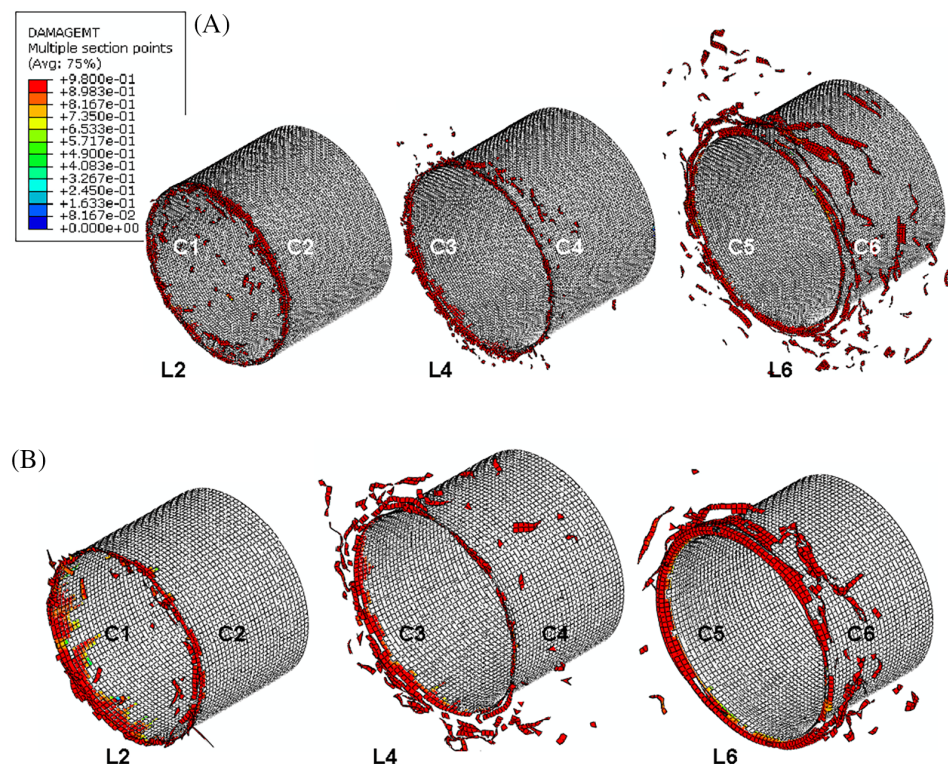


FIGURE B3 Damage and delamination of composite layers L2, L4 and L6 in angle-ply models, $V_0 = 10$ m/s, $G = 46$ kg, $t = 0.0028$ s; (A) Mesh size 0.75 mm, crush distance 25.34 mm; (B) Mesh size 1.25 mm, crush distance 25.46 mm [Color figure can be viewed at wileyonlinelibrary.com]

difference between the crushing distances of the two models at this particular time.

The damage of the 0° layers (2, 4, and 6) are illustrated in Figure B3 representing the composite layers together with the inserted epoxy layers modelling the delamination. It is evident that the delaminated sections of the models shown in Figure B2 at comparable crush distances are somewhat larger for the model with 1.25 mm element size which results in a lower force shown in Figure B1(A). The mesh sensitivity analysis confirms that the proposed FE model for inter-laminar damage is capable of predicting accurately the response of GFRP tubes to a low-velocity axial impact for

sufficiently small elements when compromising between the computational cost and accuracy.

APPENDIX C: Comparisons between the proposed model and a surface-based cohesive model

Force-displacement curves predicted by the proposed model for delamination are compared with the results obtained when applying the surface-based cohesive model formulation (CZS) available in Abaqus.^[37] Examples are presented in Figure C1 for axial impact of cross-ply tubes with $V_0 = 7$ m/s, $G = 100$ kg (Figure C1

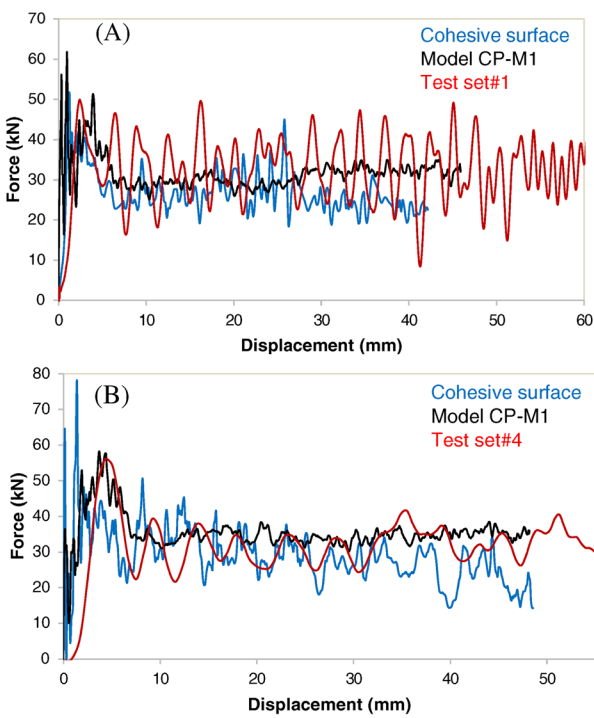
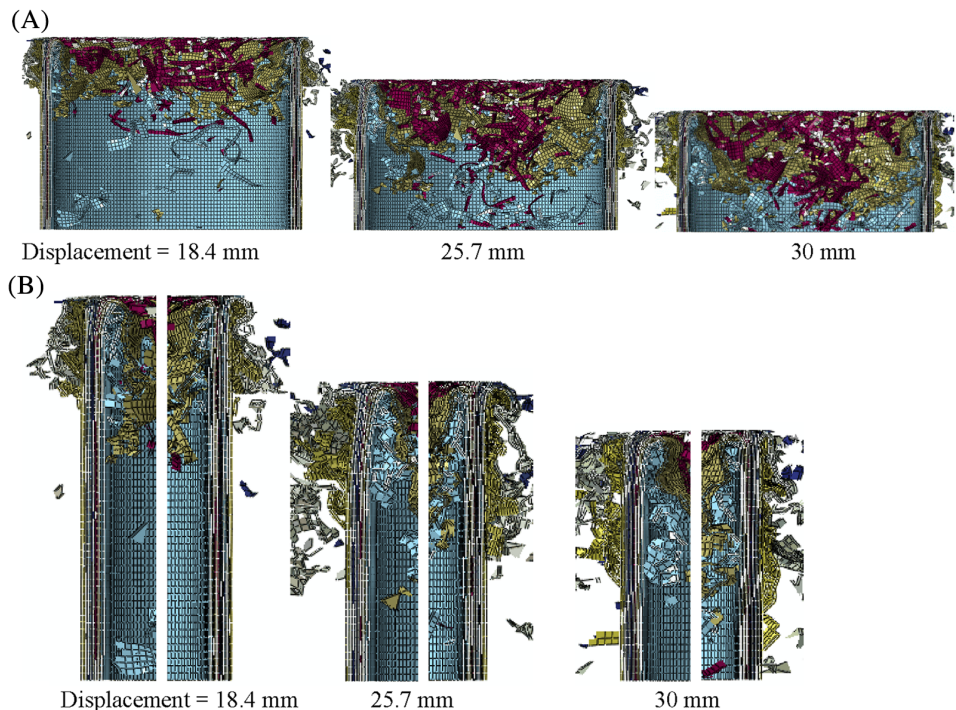


FIGURE C1 Force–displacement curves obtained experimentally (red), the predictions of the present model (black) and surface-based cohesive model (blue); (A) $V_0 = 7 \text{ m/s}$, $G = 100 \text{ kg}$; (B) $V_0 = 10 \text{ m/s}$, $G = 49 \text{ kg}$ [Color figure can be viewed at wileyonlinelibrary.com]

TABLE C1 Parameters used in the traction separation law for the cohesive surface interaction

$t_n^{\max} (\text{MPa})$	$t_s^{\max} = t_t^{\max} (\text{MPa})$	α	$G_{IC} (\text{N/mm})$	$G_{IIC} = G_{IIIc} (\text{N/mm})$
65	72	1	0.39	2.85

FIGURE C2 Deformed shapes of the cross-ply tube using a surface-based-cohesive model, $V_0 = 10 \text{ m/s}$, $G = 46 \text{ kg}$. (A) A half tube at subsequent crushing distances; (B) Enlarged views of the tube walls [Color figure can be viewed at wileyonlinelibrary.com]



(A)) and $V_0 = 10 \text{ m/s}$, $G = 49 \text{ kg}$ (Figure C1(B)). The geometric and material characteristics of the composite layers are the same as those described in the main body of the paper. The traction-separation uncoupled behavior is used with stiffness coefficients K_n , K_s , K_t which are the normal and tangential stiffness components; $K_n = K_s = K_t = 10^5 \text{ N/mm}^3$ ^[48].

Quadratic stress criterion is used for damage initiation

$$\left(\frac{\langle t_n \rangle}{t_n^{\max}} \right)^2 + \left(\frac{t_s}{t_s^{\max}} \right)^2 + \left(\frac{t_t}{t_t^{\max}} \right)^2 = 1$$

where t_n is the inter-laminar normal contact stress in the pure normal mode; t_s and t_t are the shear contact stresses along the first and shear directions, respectively. The energy-based damage evolution criterion is applied as a function of mode mix in the power-low form

$$\left(\frac{G_I}{G_{IC}} \right)^\alpha + \left(\frac{G_{II}}{G_{IIC}} \right)^\alpha + \left(\frac{G_{III}}{G_{IIIc}} \right)^\alpha = 1$$

where G_{IC} , G_{IIC} and G_{IIIc} refer to the critical fracture energies required to cause failure in the normal, the first, and the second shear directions, respectively. The

composite layers can contact again after delamination according to the general contact algorithm. The parameters for the traction separation law for the cohesive surface interaction used in the simulations are given in Table C1.

The comparison between the force–displacement curves in Figure C1 shows that the two numerical models resemble the experimental test results for axial displacements smaller than approximately 25 mm. For larger displacements, however, the force-displacement curves predicted by the CZS model corresponding to both loading cases start to deviate from the experimental curves predicting lower values. The cohesive surface-based approach predicts larger delamination areas between the composite layers which are the reason for the lower local bending stiffness of the tube section. Deformed shapes of

a cross-ply tube under an impact with $V_0 = 10$ m/s, $G = 49$ kg are presented in Figure C2 for three values of the axial displacements. The enlarged images of the tube walls in the cut view presented in Figure C2(B) show that delamination is spread at a larger distance from the impacted end in comparison with the tested tubes where delamination developed at a distance comparable with the tube thickness. The reduced local bending stiffness of the tube initiates additional buckling modes as shown in Figure C2(A),(B) for axial displacement of 25.7 mm. This phenomenon contributes to further rapid development of delamination and reduction of the tube strength resulting in smaller axial forces (Figure C1). It should be noted that an increase in the critical fracture energies can “delay” but not eliminate the development of buckling during the response.